

# Theory of ultrafast nonlinear optics of Coulomb-coupled semiconductor quantum dots: Rabi oscillations and pump-probe spectra

J. Danckwerts, K. J. Ahn, J. Förstner, and A. Knorr

*Institut für Theoretische Physik, AG Nichtlineare Optik und Quantenelektronik, Technische Universität Berlin, Hardenbergstraße 36, PN 7-1 10623 Berlin, Germany*

(Received 19 October 2005; published 18 April 2006)

We investigate the optical properties of a Coulomb-coupled double-quantum dot system excited by coherent light pulses. Basic effects of Coulomb coupling regarding linear and nonlinear optical processes are discussed. By numerically solving the Heisenberg equation of motion we are able to present the temporal evolution of the system's density matrix for a wide range of coupling parameters. The two main coupling effects in dipole approximation, biexcitonic shift and Förster energy transfer, are investigated and their qualitative and quantitative influence on absorption spectra, Rabi oscillations, and single- and two-pulse excitation is discussed. We present simulated differential transmission spectra to allow for comparison with recent experimental studies.

DOI: [10.1103/PhysRevB.73.165318](https://doi.org/10.1103/PhysRevB.73.165318)

PACS number(s): 78.67.Hc, 73.21.La, 73.20.Mf, 03.67.Lx

## I. INTRODUCTION

Semiconductor quantum dots have been intensively studied due to the various ways of using them in electro-optical devices such as lasers or light-emitting diodes (LED's).<sup>1</sup> Apart from possible applications they represent important model systems of three-dimensional electron confinement in semiconductors. With regard to optical properties they combine atomiclike behavior like discrete spectra with that of bulk semiconductors like excitonic features.<sup>2</sup> Furthermore, the discrete energy states of electrons confined in quantum dots also mark them as promising candidates for basic building blocks of quantum computers. There exists a wide range of suggestions how to identify quantum mechanical states in a quantum dot as qubits and how to utilize interaction mechanisms to implement basic quantum operations.<sup>3-7</sup> Especially small optical linewidths at low temperatures<sup>8</sup> and the possibility of coherent optical control of single quantum dots via Rabi oscillations<sup>9-11</sup> seem to make quantum information applications using semiconductor quantum dots feasible. One of the most promising proposals of an all-optical implementation of quantum information processing involves Coulomb coupled quantum dots driven by coherent light pulses.<sup>7</sup>

Therefore an investigation of the dynamical behavior of two coupled quantum dots under the influence of coherent laser pulses, taking into account all effects of the Coulomb interaction between the dots, is of special importance for quantum information applications. Previous theoretical studies have shown how the CNOT operation can be implemented in a two-quantum dot system if the biexcitonic shift is enhanced with additional fields.<sup>12</sup> There, the Förster transfer was assumed to be negligible. Other efforts have been directed at comparing methods of generating entangled states in the system and calculating the Coulomb matrix elements for different quantum dot geometries.<sup>6</sup>

In this paper, we present a theoretical analysis of the basic properties of a quantum dot system consisting of two quantum dots that are coupled via Coulomb interaction and simultaneously excited by coherent light pulses. The Coulomb in-

teraction is treated in dipole approximation, leading to the known effects of a biexcitonic energy shift and Förster energy transfer. The strength of the corresponding coupling matrix elements is known to depend strongly on parameters like the quantum dot material, structure, and external parameters like, for example, electric fields.<sup>6</sup> We study the influence of the different coupling effects on coherent phenomena such as Rabi oscillations<sup>13</sup> and pulsed excitation of the system for a wide range of parameters, thereby including different geometries and quantum dot types like interface quantum dots<sup>14</sup> or self-assembled quantum dots.<sup>1,15</sup> Furthermore, a pump-probe setup is modeled to determine the effects of Coulomb coupling on nonlinear optical spectra obtainable by differential transmission spectroscopy.<sup>16</sup> Knowledge of the relative impact of different interaction parameters on the spectra is important for the interpretation of experimental results such as Ref. 16. Therefore the differential transmission spectra are calculated for different regimes of Coulomb coupling where either one of the two coupling effects can be neglected or both have to be taken into account.

The paper is organized as follows: first, we introduce the theoretical framework, specifying the Hamiltonian and the way the Coulomb interaction is treated. Then, the equations of motion in rotating-wave approximation are derived and solved numerically. Results regarding coherent excitation of the system, especially Rabi oscillations, energy transfer between the dots, and differential transmission spectra, are discussed.

## II. HAMILTONIAN

The system described here consists of two semiconductor quantum dots. The electrons confined in these quantum dots interact both with the external coherent light field and with each other via Coulomb interaction. Restricting the investigation to the low-temperature regime, the coupling to phonons of the surrounding semiconductor material is omitted here.<sup>17,18</sup> It is assumed that there is no overlap between the electron wave functions of different quantum dots; i.e., no electronic coupling or tunneling occurs. The approach to

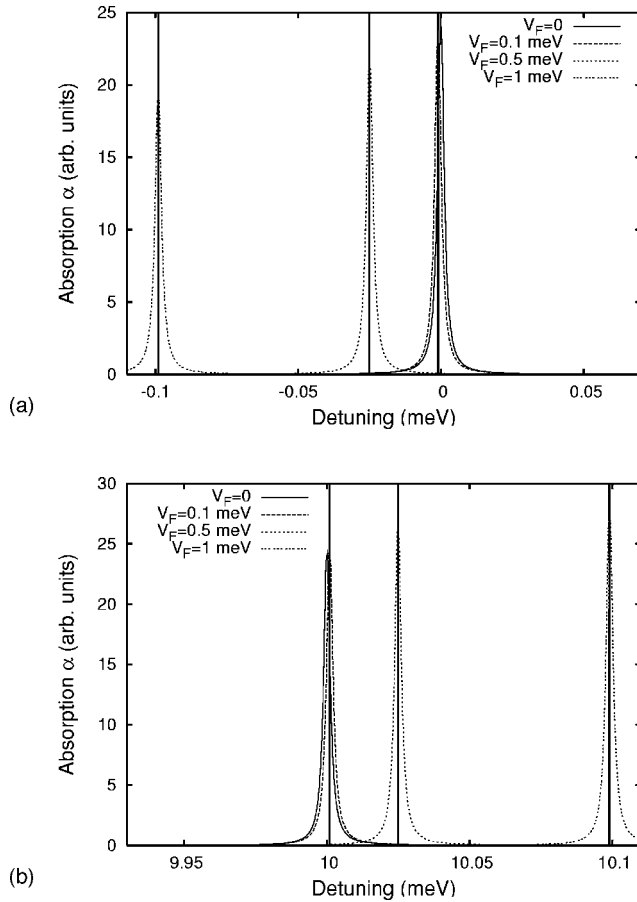


FIG. 1. Nonidentical quantum dots: linear absorption spectra versus detuning to the lower quantum dot resonance for the lower-energy quantum dot (top) and higher-energy quantum dot (bottom), calculated for different values of the Förster matrix element. The corresponding analytically calculated positions of the absorption lines are indicated as vertical lines.

map the full many-body problem on a discrete level scheme for the strongly confined excitons is supported by various experimental and theoretical studies; for instance, see Ref. 19. In our investigation, we want to focus on the case of optical pulses resonant to the lowest possible electronic transition between valence and conduction band states in each of the quantum dot—i.e., quantum dots as two-level systems. For quantum dots smaller than the exciton Bohr radius and resonant excitation of the energetically lowest excited state it is common to model the quantum dot system as a two-level system.<sup>20</sup> Such a model system can be realized by using spectrally narrow polarized pulses to avoid single-dot biexciton excitation and the excitation of higher confined or even continuum states.

The electrons in the individual quantum dots are described using the effective mass approximation.<sup>21</sup> The Heisenberg field operators  $\phi^\dagger, \phi$  are products of envelope functions  $\xi_\lambda$  and Bloch functions  $u_\lambda$  at wave number  $k=0$  having the form  $\phi_{\lambda,n}^\dagger = \xi_{\lambda,n} u_{\lambda,n} a_{\lambda,n}^\dagger$ , with  $a_{\lambda,n}^\dagger$  being the creation operator and  $a_{\lambda,n}$  the destruction operator of an electron in level  $\lambda$  in the  $n$ th quantum dot. The Hamiltonian  $H_e$  for noninteracting electrons with energy levels  $\epsilon_i$  then reads as

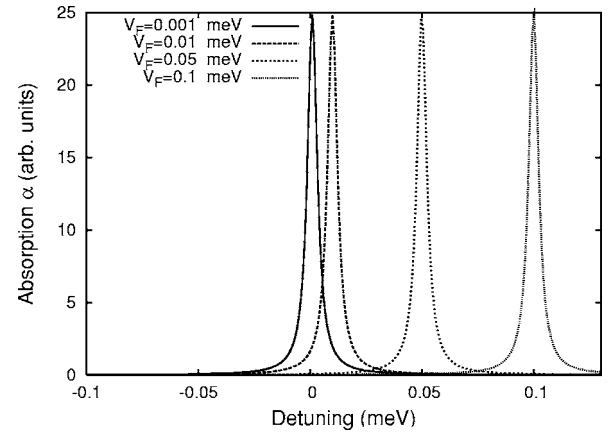


FIG. 2. Identical quantum dots: linear absorption spectra versus detuning to the lower quantum dot resonance for different values of the Förster matrix element and a radiative damping of  $\gamma = (500 \text{ ps})^{-1}$ . There is just one resonance, since the lower resonance cannot be excited optically.

$$H_e = \sum_{\lambda,n} \epsilon_{\lambda,n} a_{\lambda,n}^\dagger a_{\lambda,n}. \quad (1)$$

Since we are interested in optical transitions between conduction ( $\lambda=c$ ) and valence band ( $\lambda=v$ ), we restrict the investigation to two-level-systems without taking spin degeneracy in each quantum dot into account (fixed circular polarization).

The electron-light interaction is treated in two different ways in our work: excitation of the system with a coherent laser source is treated in a semiclassical approach, where the electric field is described as a nonquantized vector field, while we use the completely quantized interaction Hamiltonian to include at least radiative damping in our calculations to provide a source of dephasing for the excited zero-phonon line at low temperatures.<sup>17</sup> The semiclassical part of the Hamiltonian in dipole approximation is given by

$$H_{e-l} = -\mathbf{E}(t) \cdot \mathbf{d}_{cv} \sum_n (a_{c,n}^\dagger a_{v,n} X_{cv,n} + a_{v,n}^\dagger a_{c,n} X_{vc,n}), \quad (2)$$

with the classical light field  $\mathbf{E}(t)$ , the dipole matrix element  $\mathbf{d}_{cv} = V_u^{-1} \int d^3\mathbf{r} u_c^*(\mathbf{r}) \mathbf{e} \mathbf{r} u_v(\mathbf{r})$  for the transition between the valence and conduction bands, and the volume of the unit cell,  $V_u$ . The spatial extension of the quantum dots results in factors  $X_{ij,n} = \int_{V_{\text{dot}}} \xi_{i,n}^*(\mathbf{r}) \xi_{j,n}(\mathbf{r}) d\mathbf{r}$  in the Hamiltonian.

The quantized electron-photon interaction is given by

$$H_{e-ph} = \sum_{n,k} G_{cv,k} [a_{c,n}^\dagger a_{v,n} (c_k + c_k^\dagger) + a_{v,n}^\dagger a_{c,n} (c_{-k} + c_{-k}^\dagger)], \quad (3)$$

where  $c_k$  ( $c_k^\dagger$ ) are the destruction (creation) operators of photons of mode  $k$  (dispersion  $\omega_k$ ) and  $G_{cv,k}$  is the interaction matrix element. Here, the photons are treated as a heat bath, with the Hamiltonian of the free photons given by  $H_{ph} = \sum_k \hbar \omega_k c_k^\dagger c_k$ .

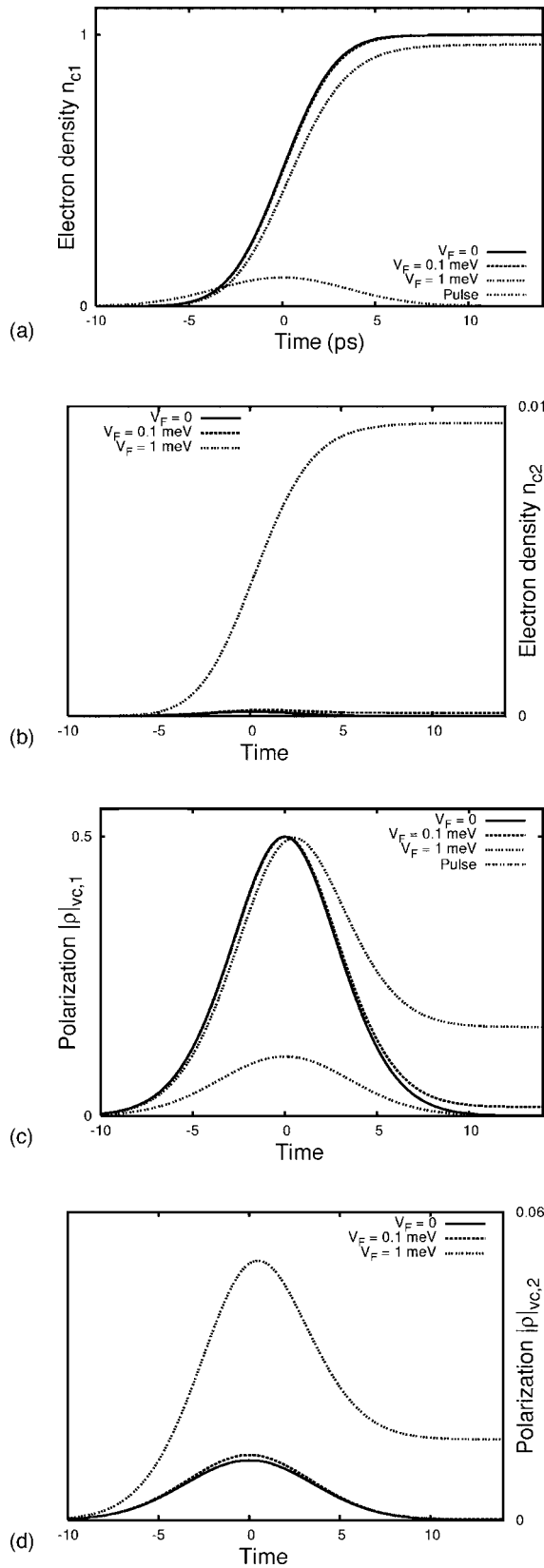


FIG. 3. Resonant excitation of the lower resonance: temporal evolution of electron density (top) and polarization (bottom) of the lower-energy (left) and higher-energy (right) quantum dot during excitation with a 5-ps  $\pi$  pulse.

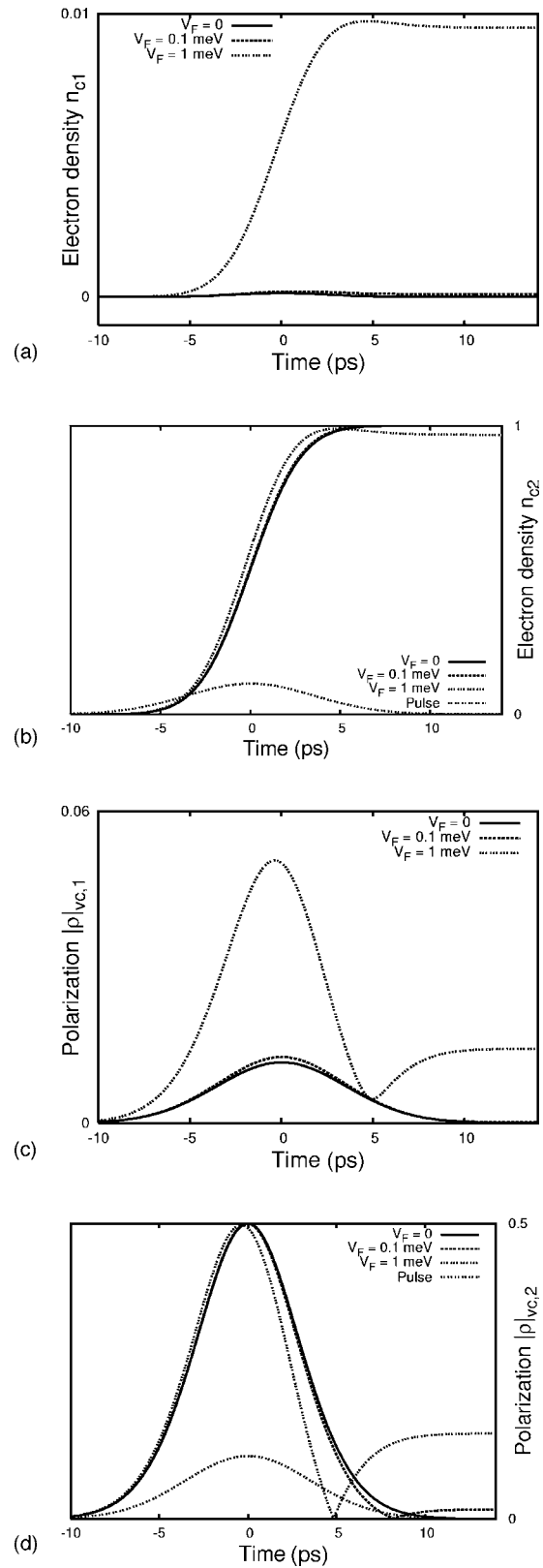


FIG. 4. Resonant excitation of the higher resonance: temporal evolution of electron density (top) and polarization (bottom) of the lower-energy (left) and higher-energy (right) quantum dots during excitation with a 5-ps  $\pi$  pulse without radiative damping.

The Coulomb interaction manifests itself as an additional term  $H_c$  in the Hamiltonian which in second quantization picture can be written as

$$H_c = \frac{1}{2} \sum_{a,b,c,d} V_{abcd} a_{\lambda_a n_a}^\dagger a_{\lambda_b n_b}^\dagger a_{\lambda_c n_c} a_{\lambda_d n_d}, \quad (4)$$

with the Coulomb matrix element

$$H_{c,abcd} = \frac{e^2}{8\pi\epsilon_0} \int \frac{\xi_{\lambda_a n_a}^*(\mathbf{r}) \xi_{\lambda_b n_b}^*(\mathbf{r}') \xi_{\lambda_c n_c}(\mathbf{r}) \xi_{\lambda_d n_d}(\mathbf{r}')}{|\mathbf{r} - \mathbf{r}'|} \times u_{\lambda_a n_a}^*(\mathbf{r}) u_{\lambda_b n_b}^*(\mathbf{r}') u_{\lambda_c n_c}(\mathbf{r}) u_{\lambda_d n_d}(\mathbf{r}') d^3\mathbf{r} d^3\mathbf{r}'. \quad (5)$$

The total Hamiltonian of the system is obtained by summarizing the part of the noninteracting electrons and photons and the interaction contributions:

$$H = H_e + H_{ph} + H_{e-l} + H_{e-ph} + H_c. \quad (6)$$

### III. DENSITY MATRIX ELEMENTS

In the second-quantization picture an electron state  $|i\rangle$  is given by  $|i\rangle = a_i^\dagger |0\rangle$ , where  $|0\rangle$  is the vacuum state and  $a_i^\dagger$  the creation operator for an electron in state  $i$ . The basis for the single-electron state is spanned by the set  $\{|i\rangle\}$ . The density matrix elements  $\rho_{ij} = \langle i | \rho | j \rangle$  of the single electrons in quantum dot  $n$  are given by the expectation values of destruction and creation operator products:

$$\rho_{ij,n} = \langle a_{j,n}^\dagger a_{i,n} \rangle, \quad i, j \in \{c, v\}. \quad (7)$$

We refer to the diagonal elements as electron population densities  $n_{i,n} = \langle a_{i,n}^\dagger a_{i,n} \rangle$  and to the nondiagonal elements as microscopic coherences or microscopic polarizations  $\rho_{cv,n} = \langle a_{v,n}^\dagger a_{c,n} \rangle$ . For the two-level-system, according to their definition, the electron operators fulfill the identity

$$a_{c,n}^\dagger a_{c,n} + a_{v,n}^\dagger a_{v,n} = \mathbf{1}_n, \quad (8)$$

where  $\mathbf{1}_n$  denotes the identity acting on the states of quantum dot  $n$ .

For a system of two electrons, the basis states are the tensor products of the single-electron basis states:  $|ij\rangle = |i\rangle \otimes |j\rangle$ . The density matrix elements are then given by four-operator expectation values:

$$\rho_{kl ij, n_1 n_2} = \langle a_{j, n_1}^\dagger a_{i, n_2}^\dagger a_{l, n_2} a_{k, n_1} \rangle. \quad (9)$$

By using Eq. (8) one can see that two-operator expectation values are obtained from four-operator expectation values by

$$\langle a_{i, n_1}^\dagger a_{c, n_2}^\dagger a_{c, n_2} a_{j, n_1} \rangle + \langle a_{i, n_1}^\dagger a_{v, n_2}^\dagger a_{v, n_2} a_{j, n_1} \rangle = \langle a_{i, n_1}^\dagger a_{j, n_1} \rangle. \quad (10)$$

This identity shows that the density matrix elements of an electron in the first quantum dot result from the full density matrix of the system by taking the partial trace over the second quantum dot and vice versa.

In the following considerations we fix  $n_1=1$ ,  $n_2=2$  in the density matrix elements  $\rho_{kl ij, n_1 n_2}$ , Eq. (11). Therefore, the indices  $n_1, n_2$  are omitted in the equations.

Optical excitation phenomena are described via microscopic coherences, Eq. (7), from which the macroscopic polarization  $P = \sum_n d_{cv} \rho_{cv, n} + d_{cv} \rho_{cv, n}^*$  of the system and the linear absorption spectrum  $\alpha(\omega)$  can be obtained by

$$\alpha(\omega) \propto \text{Im}[P(\omega)/E(\omega)]. \quad (11)$$

### IV. DIPOLE APPROXIMATION OF COULOMB MATRIX ELEMENTS

The Coulomb interaction potential is treated in a dipole approximation. For this we perform a Taylor series expansion of the  $1/|\mathbf{r} - \mathbf{r}'|$  term in the matrix elements in Eq. (5). In doing so we introduce the reference point  $\mathbf{R}$  and the vector  $\tilde{\mathbf{r}} = \mathbf{r} - \mathbf{R}$ . The wave functions consist of two terms, one (the Bloch function part  $u_\lambda$ ) varying on the scale of the unit cell and another (the envelope function  $\xi_\lambda$ ) varying on the mesoscopic scale of the quantum dot. Therefore, for evaluating the Taylor expansion two different length scales (corresponding to the two wave functions) have to be considered:

(i) Long-range expansion: the reference point  $\mathbf{R} = \mathbf{R}_0$  ( $\mathbf{R} = \mathbf{R}_0$ ) lies within the first (second) quantum dot;  $\tilde{\mathbf{r}}_0 = \mathbf{r} - \mathbf{R}_0$  varies on the mesoscopic length scale within the quantum dot radius. The variation in the unit cell is ignored. The resulting form of the matrix elements is

$$V_{abcd} = \frac{1}{8\pi\epsilon} \int d^3\tilde{\mathbf{r}}_0 d^3\tilde{\mathbf{r}}'_0 \left[ \frac{1}{R_{12}} - \frac{1}{R_{12}^3} \mathbf{R}_{12} e^{i(\tilde{\mathbf{r}}_0 + \tilde{\mathbf{r}}'_0)} + \frac{e\tilde{\mathbf{r}}_0 \cdot e\tilde{\mathbf{r}}'_0}{|R_{12}|^3} - 3 \frac{(\mathbf{R}_{12} \cdot e\tilde{\mathbf{r}}_0)(\mathbf{R}_{12} \cdot e\tilde{\mathbf{r}}'_0)}{|R_{12}|^5} \right] \cdot \xi_{\lambda_a n_a}^*(\tilde{\mathbf{r}}_0) \xi_{\lambda_b n_b}^*(\tilde{\mathbf{r}}'_0) \xi_{\lambda_c n_c}(\tilde{\mathbf{r}}_0) \xi_{\lambda_d n_d}(\tilde{\mathbf{r}}'_0) \delta_{\lambda_a \lambda_c} \delta_{\lambda_b \lambda_d}. \quad (12)$$

Here we have introduced  $R_{12} = |\mathbf{R}_0 - \mathbf{R}_0'|$  as the quantum dot distance. The form of  $V_{abcd}$  is analogous to the dipole-interaction energy term of classical electrodynamics. The orthogonality of the Bloch functions has caused a band index diagonality, so this expansion results in diagonal matrix elements.

In the following we will restrict the discussion to the dipole-dipole-interaction term (\*):

$$V_{abcd} = \frac{1}{8\pi\epsilon} \int d^3\tilde{\mathbf{r}}_0 d^3\tilde{\mathbf{r}}'_0 \left( \frac{e\tilde{\mathbf{r}}_0 \cdot e\tilde{\mathbf{r}}'_0}{|R_{12}|^3} - 3 \frac{(\mathbf{R}_{12} \cdot e\tilde{\mathbf{r}}_0)(\mathbf{R}_{12} \cdot e\tilde{\mathbf{r}}'_0)}{|R_{12}|^5} \right) \times \xi_{\lambda_a n_a}^*(\tilde{\mathbf{r}}_0) \xi_{\lambda_b n_b}^*(\tilde{\mathbf{r}}'_0) \xi_{\lambda_c n_c}(\tilde{\mathbf{r}}_0) \xi_{\lambda_d n_d}(\tilde{\mathbf{r}}'_0) \delta_{\lambda_a \lambda_c} \delta_{\lambda_b \lambda_d}. \quad (13)$$

(ii) Short-range expansion: the reference point  $\mathbf{R} = \mathbf{R}_G$  is a lattice vector and the vector  $\tilde{\mathbf{r}}_G$  varies on the length scale of the unit cell. In the unit cells the envelope functions have a constant value. This leads to the following expression for dipole-dipole term of the matrix elements:

$$V_{abcd} = \frac{1}{8\pi\epsilon} \int d^3\mathbf{R}_G d^3\mathbf{R}'_G \left( \frac{\mathbf{d}_{\lambda_a\lambda_c} \cdot \mathbf{d}_{\lambda_b\lambda_d}}{|\mathbf{R}_G - \mathbf{R}'_G|^3} - 3 \frac{(\mathbf{R}_G - \mathbf{R}'_G) \cdot \mathbf{d}_{\lambda_a\lambda_c} (\mathbf{R}_G - \mathbf{R}'_G) \cdot \mathbf{d}_{\lambda_b\lambda_d}}{|\mathbf{R}_G - \mathbf{R}'_G|^5} \right) \times \xi_{\lambda_a n_a}^*(\mathbf{R}_G) \xi_{\lambda_b n_b}^*(\mathbf{R}') \xi_{\lambda_c n_a}(\mathbf{R}_G) \xi_{\lambda_d n_b}(\mathbf{R}'). \quad (14)$$

These matrix elements are nondiagonal since the dipole matrix elements  $\mathbf{d}_{\lambda_1\lambda_2}$  can be assumed to be zero for identical band indices.

Before a numerical approach to the full interacting system, we develop some analytical insight into the eigenstates and eigenenergies of the coupled quantum dot system.

## V. COULOMB INTERACTIONS IN THE TWO-ELECTRON BASIS

For a matrix representation of the Hamiltonian, following the formalism of Lovett *et al.*,<sup>6</sup> we define the excited ( $|1\rangle$ ) and ground ( $|0\rangle$ ) electron states as a basis in each quantum dot. In our two-level system they correspond to the existence

of nonexistence of an electron-hole pair in this quantum dot. The basis for the two electron states can then be represented by the set ( $|00\rangle, |10\rangle, |01\rangle, |11\rangle$ ). The matrix elements  $V_{ijkl} = \langle ij|H_c|kl\rangle$  of the Coulomb operator then form the interaction matrix

$$V = \begin{pmatrix} V_{0000} & 0 & 0 & 0 \\ 0 & V_{1010} & V_{0110} & 0 \\ 0 & V_{1001} & V_{0101} & 0 \\ 0 & 0 & 0 & V_{1111} \end{pmatrix}. \quad (15)$$

Here, we have assumed  $V_{1100} = V_{0011} = 0$ , since this element represents a Coulomb-induced transition between the states  $|00\rangle$  and  $|11\rangle$ , which violates energy conservation. Also, when applying the rotating-wave approximation (cf. Sec. VII) the terms caused by this matrix element do not contribute to the equations of motion. In the following we refer to the diagonal elements  $V_{ijij}$  as  $V_{ij}$  and to the nondiagonal term  $V_{0110}$  ( $=V_{1001}$ , assuming  $V_{0110}$  is real) as  $V_F$ , the Förster matrix element, since it represents the Förster energy transfer.

The Hamiltonian matrix without electron-light interaction terms is then given by

$$H_e + H_{e-c} = \begin{pmatrix} \hbar\omega_0 + V_{00} & 0 & 0 & 0 \\ 0 & \hbar\omega_0 + \hbar\omega_1 + V_{10} & V_F & 0 \\ 0 & V_F & \hbar\omega_0 + \hbar\omega_2 + V_{01} & 0 \\ 0 & 0 & 0 & \hbar\omega_0 + \hbar\omega_1 + \hbar\omega_2 + V_{11} \end{pmatrix}. \quad (16)$$

Here, we introduced  $\hbar\omega_0 = \epsilon_{v1} + \epsilon_{v2}$ ,  $\hbar\omega_1 = \epsilon_{c1} - \epsilon_{v1}$ , and  $\hbar\omega_2 = \epsilon_{c2} - \epsilon_{v2}$ .

The main effect caused by the Coulomb interaction can be seen if this Hamiltonian is diagonalized. The corresponding eigenvalues ( $\lambda_i$ ) and eigenvectors ( $|\Psi_i\rangle$ ) are

$$|\Psi_1\rangle = |00\rangle, \quad \lambda_1 = \hbar\omega_0 + V_{00},$$

$$|\Psi_2\rangle = (c_1|10\rangle - c_2|01\rangle), \quad \lambda_2 = \hbar\omega_0 + \hbar\omega_1 + V_{10} + \frac{1}{2}(\Delta - \sqrt{\Delta^2 + 4V_F^2}),$$

$$|\Psi_3\rangle = (c_2|10\rangle + c_1|01\rangle), \quad \lambda_3 = \hbar\omega_0 + \hbar\omega_1 + V_{10} + \frac{1}{2}(\Delta + \sqrt{\Delta^2 + 4V_F^2}),$$

$$|\Psi_4\rangle = |11\rangle, \quad \lambda_4 = \hbar\omega_0 + \hbar\omega_1 + \hbar\omega_2 + V_{11}, \quad (17)$$

where  $\Delta = \hbar\omega_2 - \hbar\omega_1 + V_{01} - V_{10}$  is the difference of the single-excitonic energies in the quantum dots ( $\omega_2 > \omega_1$ ). The factors  $c_1, c_2$  depend on the matrix elements.

$$c_1 = (\Delta + \sqrt{\Delta^2 + 4V_F^2})[4V_F^2 + (\Delta + \sqrt{\Delta^2 + 4V_F^2})^2]^{-1/2}, \quad (18)$$

$$c_2 = 2V_F[4V_F^2 + (\Delta + \sqrt{\Delta^2 + 4V_F^2})^2]^{-1/2}. \quad (19)$$

The diagonalization shows how the two Coulomb coupling effects arise: due to the interaction the old single-exciton basis states ( $|01\rangle$  and  $|10\rangle$ ) superimpose to form the new states  $|\Psi_2\rangle$  and  $|\Psi_3\rangle$ . They represent states where the excitation is not completely localized in one of the two dots anymore. As a consequence, if the system is prepared in, for example, the state  $|\phi\rangle = |01\rangle$ , in the new basis this state is a superposition of the states  $|\Psi_2\rangle$  and  $|\Psi_3\rangle$ :  $|\phi(0)\rangle = a|\Psi_2\rangle + b|\Psi_3\rangle$  with  $|a|^2 + |b|^2 = 1$ . Due to the differing energies  $\lambda_2, \lambda_3$ , the state becomes time dependent:  $|\phi(t)\rangle = ae^{(-i\lambda_2/\hbar)t}|\Psi_2\rangle + be^{(-i\lambda_3/\hbar)t}|\Psi_3\rangle$ . In this case the exciton energy oscillates between the first and second quantum dots: Förster energy transfer occurs.

As a consequence, the excitation energies for the creation of a single exciton change: the energy needed to create the lower-energy exciton is given by  $\hbar\omega_1 + V_{10} - V_{00} + \frac{1}{2}(\Delta - \sqrt{\Delta^2 + 4V_F^2})$  instead of  $\hbar\omega_1$  and the one needed to create the higher-energy exciton is given by  $\hbar\omega_1 + V_{10} + \frac{1}{2}(\Delta$

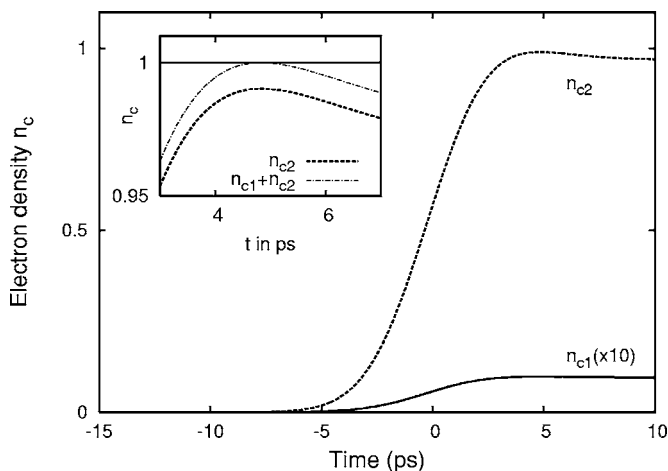


FIG. 5. Time evolution of electron densities of both quantum dots during excitation with a 5-ps  $\pi$  pulse that is resonant to the higher resonance. The inset shows the electron density of the higher-energy quantum dot and the sum of both densities around the maximum.

$+\sqrt{\Delta^2+4V_F^2}$ ) instead of  $\hbar\omega_2$ . In linear absorption spectra the distance between the two lines of different quantum dots increases with rising  $V_F$ , as will be shown in Sec. VI.

Furthermore, the energy level of the state  $|11\rangle$  changes; the energy needed to excite a second exciton in the system may be different from the energy needed to create that exciton in the absence of the first. This difference is called the biexcitonic shift, given by  $\Delta E = V_{11} - V_{10} - V_{01} + V_{00}$ .

### VI. HAMILTONIAN MATRIX INCLUDING ELECTRON-LIGHT INTERACTION

The analytical diagonalization discussed above results if one neglects the electron light interaction term in the Hamiltonian. When including  $H_{e-l}$ , the full Hamiltonian is not diagonal in the basis  $\{|\Psi_i\rangle\}$  anymore. Displayed in the basis  $\{|\Psi_i\rangle\}$ , the full Hamiltonian has the form

$$H = \begin{pmatrix} \lambda_1 & \Omega A & \Omega B & 0 \\ \Omega A & \lambda_2 & 0 & \Omega B \\ \Omega B & 0 & \lambda_3 & \Omega A \\ 0 & \Omega B & \Omega A & \lambda_4 \end{pmatrix}, \quad (20)$$

with the Rabi frequency  $\Omega = \tilde{\mathbf{E}}(t) \cdot \mathbf{d}_{cv} / \hbar$  and the normalization factors

$$A = \frac{-2V_F + \Delta + \sqrt{\Delta^2 + 4V_F^2}}{\sqrt{2}\sqrt{4V_F^2 + \Delta(\Delta + \sqrt{\Delta^2 + 4V_F^2})}}, \quad (21)$$

$$B = \frac{2V_F + \Delta + \sqrt{\Delta^2 + 4V_F^2}}{\sqrt{2}\sqrt{4V_F^2 + \Delta(\Delta + \sqrt{\Delta^2 + 4V_F^2})}}. \quad (22)$$

This Hamiltonian has the same structure as that for the uncoupled four-level system interacting with a coherent light field, apart from the occurrence of the factors  $A$  and  $B$ . Yet

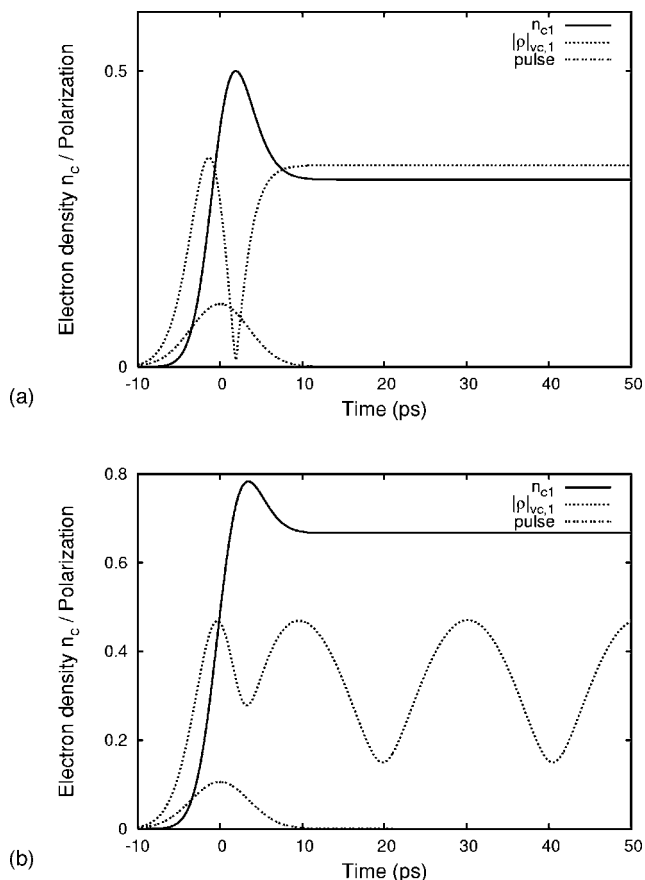


FIG. 6. Single-pulse excitation with a 5-ps  $\pi$  pulse of identical quantum dots. Top: strong Coulomb coupling ( $V_F=0.1$  meV,  $V_{11}=5$  meV). Both density and polarization are constant after the excitation. Bottom: weak Coulomb coupling ( $V_F=0.1$  meV,  $V_{11}=0$ ). The polarization oscillates, the density after the excitation is constant.

the factors  $A$  and  $B$  in the Hamiltonian represent a rescaling of the Rabi frequency  $\Omega$ , thus changing the pulse area that is necessary to obtain a full Rabi oscillation in the new level scheme. This renormalization results in a change of the period of Rabi oscillations in the system. If the resonance energies differ, the period of the higher resonance is lowered, while the one of the lower resonance is extended.

For identical quantum dots ( $\Delta=0$ ) the factor  $A$  vanishes, while the factor  $B$  has the value  $B=\sqrt{2}$ , representing a Rabi oscillation whose period is extended by the factor  $\sqrt{2}$ . The basis states in this case have the form

$$|\Psi_2\rangle = \frac{1}{\sqrt{2}}(|01\rangle - |10\rangle), \quad (23)$$

$$|\Psi_3\rangle = \frac{1}{\sqrt{2}}(|01\rangle + |10\rangle). \quad (24)$$

The transition energies for the transition from the ground state  $|\Psi_1\rangle$  to the single-excitonic states  $|\Psi_2\rangle, |\Psi_3\rangle$  are given by  $\lambda_{12} = \hbar\omega_1 + V_{10} - V_{00} - |V_F|$  and  $\lambda_{13} = \hbar\omega_1 + V_{10} - V_{00} + |V_F|$ , respectively, and for the transition from the single-excitonic to the biexcitonic state  $|\Psi_4\rangle$  by  $\lambda_{24} = \hbar\omega_1 + |V_F| + V_{11}$  and

$\lambda_{34} = \hbar \omega_1 - |V_F| + V_{11}$ . The vanishing factor  $A$  implies that the state  $|\Psi_2\rangle$  cannot be excited by the electric field in dipole approximation. The lower resonance resembles a dark state.<sup>22</sup> Therefore there is only one single-exciton resonance that can be optically excited for identical quantum dots.

## VII. EQUATIONS OF MOTION

The system's temporal evolution is described according to the Heisenberg equation of motion for the electron operators. We calculate the equations of motion for the population densities  $n_{i,n}$  and the microscopic coherences  $\rho_{cv,n}$  of the individual quantum dots labeled by the index  $n$ . They are coupled to the density matrix elements of the electrons in the two quantum dots  $\rho_{ijkl}$ .

The quantized electron-light interaction is treated in Markovian approximation, which results in radiative damping terms of the electronic density matrix elements. In this way we compute the radiative damping terms for all matrix elements. For the two-operator elements—i.e., the microscopic coherence and the electron density—these correspond to the usual phenomenological damping terms. The radiative damping of the four-operator matrix elements, however, has to be calculated in this way, since this cannot be obtained phenomenologically. All further impact of transversal coupling is discussed in future work. Especially, all higher photon correlations are neglected, since in our investigation the classical laser fields dominate the dynamics. Since only one electron-hole pair is excited in each quantum dot, the expectation values of six-operator terms resulting from the Coulomb interaction are zero. Therefore the associated system of equations is closed and can be solved numerically. Furthermore, the density matrix element is self-adjoint, and due to the identity, Eq. (10), the set of 20 equations can effectively be reduced to 9. Since the diagonal matrix elements solely shift the resonance energies resulting in the effect of the biexcitonic shift  $\Delta E = V_{11} - V_{10} - V_{01} + V_{00}$ , we neglect the diagonal terms except  $V_{11}$ , which then resembles the biexcitonic shift in our treatment. To apply the rotating-wave approximation (RWA) we transform into a frame rotating with the frequency  $\omega_0$ .<sup>13</sup> The transformation of the density matrix elements to the rotating frame [marked by a tilde ( $\sim$ )] is made by  $\rho_{cv,i} = \tilde{\rho}_{cv,i} e^{i\omega_0 t}$ ,  $\rho_{vcc} = \tilde{\rho}_{vcc} e^{-i\omega_0 t}$ ,  $\rho_{cvc} = \tilde{\rho}_{cvc} e^{-i\omega_0 t}$ , and  $\rho_{vcc} = \tilde{\rho}_{vcc} e^{-2i\omega_0 t}$ . The electric field is assumed to have the form  $\mathbf{E}(t) = \tilde{\mathbf{E}}(t) \cos(\omega_L t)$ . Then the set of equations in the rotating frame takes the form

$$\begin{aligned} \partial_t \tilde{\rho}_{vc,1} = & [-i(\omega_1 - \omega_0) - \gamma] \tilde{\rho}_{vc,1} - 0.5i\Omega^*(t)^*(n_{v,1} - n_{c,1}) \\ & + \left(\frac{iV_F}{\hbar}\right) (-\tilde{\rho}_{vc,2} + 2\tilde{\rho}_{ccv}^*) - 2i\frac{V_{11}}{\hbar} \tilde{\rho}_{ccv}^*, \end{aligned} \quad (25)$$

$$\begin{aligned} \partial_t \tilde{\rho}_{vc,2} = & [-i(\omega_2 - \omega_0) - \gamma] \tilde{\rho}_{vc,2} - 0.5i\Omega^*(t)^*(n_{v,2} - n_{c,2}) \\ & + \left(\frac{iV_F}{\hbar}\right) (-\tilde{\rho}_{vc,1} + 2\tilde{\rho}_{ccv}^*) - 2i\frac{V_{11}}{\hbar} \tilde{\rho}_{ccv}^*, \end{aligned} \quad (26)$$

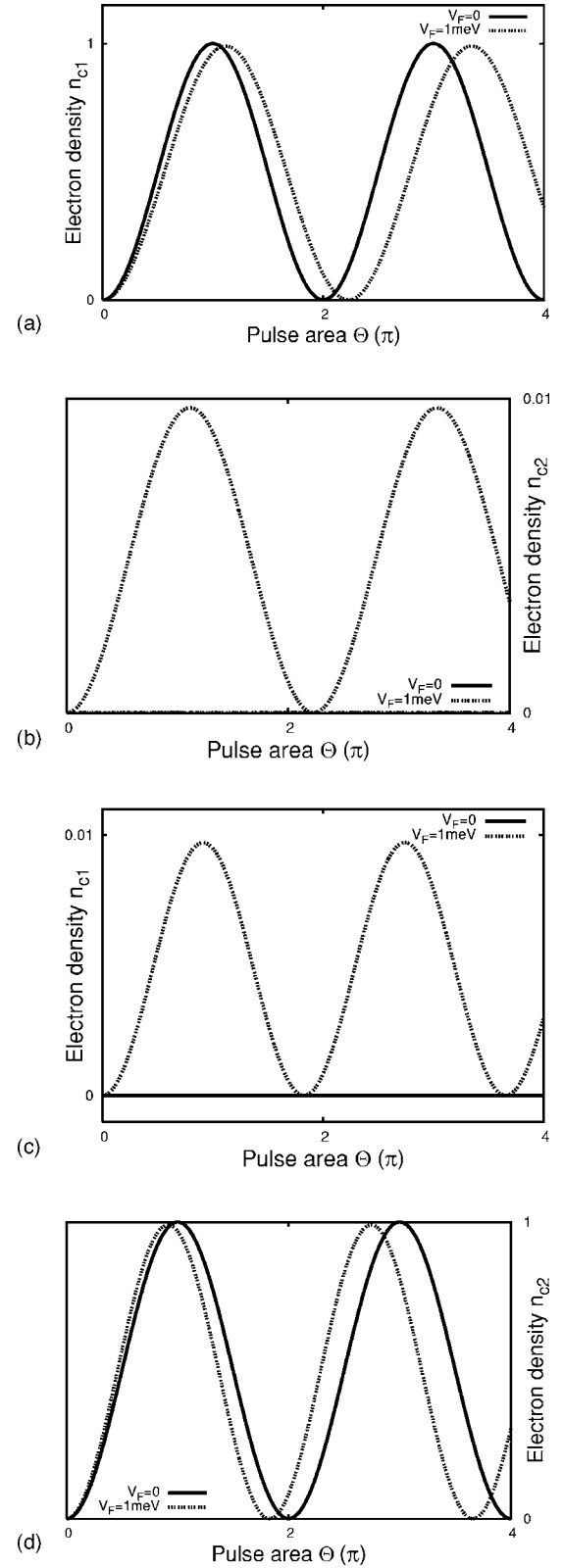


FIG. 7. Rabi oscillation of electron density with (dotted curve) and without (solid curve) Förster coupling for excitation of the lower resonance (top row) and excitation of the higher resonance (bottom row). Left: upper electron density of the lower-resonance energy quantum dot, Right: upper electron density of the higher-resonance energy quantum dot.

$$\begin{aligned} \partial_t n_{c,1} = & \gamma(-n_{c,1} - n_{c,1}^*) - 0.5i[\Omega^*(t) \tilde{\rho}_{vc,1}^* - \Omega^*(t) \tilde{\rho}_{vc,1}] \\ & - \frac{iV_F}{\hbar}(\tilde{\rho}_{cvcv} - \tilde{\rho}_{cvcv}^*), \end{aligned} \quad (27)$$

$$\begin{aligned} \partial_t n_{c,2} = & \gamma(-n_{c,2} - n_{c,2}^*) - 0.5i[\Omega^*(t) \tilde{\rho}_{vc,2}^* - \Omega^*(t) \tilde{\rho}_{vc,2}] \\ & - \frac{iV_F}{\hbar}(\tilde{\rho}_{cvcv}^* - \tilde{\rho}_{cvcv}), \end{aligned} \quad (28)$$

$$\begin{aligned} \partial_t \rho_{cccc} = & -4\gamma\rho_{cccc} - 0.5i[\Omega^*(t) (\tilde{\rho}_{cccv} + \tilde{\rho}_{cccv}^*) - \Omega^*(t) (\tilde{\rho}_{cccv}^* \\ & + \tilde{\rho}_{cccv})], \end{aligned} \quad (29)$$

$$\begin{aligned} \partial_t \tilde{\rho}_{cvcv} = & [-i(\omega_2 - \omega_1) - 2\gamma] \tilde{\rho}_{cvcv} + 0.5i[\Omega^*(t) (\tilde{\rho}_{vc,2} - 2\tilde{\rho}_{ccvc}^*) \\ & + \Omega^*(t) (-\tilde{\rho}_{vc,1} + 2\tilde{\rho}_{cccv})] + \frac{iV_F}{\hbar}(-n_{c,1} + n_{c,2}), \end{aligned} \quad (30)$$

$$\begin{aligned} \partial_t \tilde{\rho}_{cccv} = & \left[ -i \left( -\omega_1 + \omega_0 - 2\frac{V_{11}}{\hbar} \right) - 3\gamma \right] \tilde{\rho}_{cccv} + 0.5i[\Omega^*(t) \\ & \times (n_{c,2} - 2\rho_{cccc} + \tilde{\rho}_{cvcv}) - \Omega^*(t) \tilde{\rho}_{ccvv}] - \left( \frac{iV_F}{\hbar} \right) \tilde{\rho}_{ccvc}, \end{aligned} \quad (31)$$

$$\begin{aligned} \partial_t \tilde{\rho}_{ccvc} = & \left[ -i \left( -\omega_2 + \omega_0 - 2\frac{V_{11}}{\hbar} \right) - 3\gamma \right] \tilde{\rho}_{ccvc} \\ & - 0.5i\{\Omega^*(t) \tilde{\rho}_{ccvv} - \Omega^*(t) [\tilde{\rho}_{cvcv} + (n_{c,1} - 2\rho_{cccc})]\} \\ & - \left( \frac{iV_F}{\hbar} \right) \tilde{\rho}_{cccv}, \end{aligned} \quad (32)$$

$$\begin{aligned} \partial_t \tilde{\rho}_{ccvv} = & \left\{ -i \left[ -\omega_1 - \omega_2 + 2 \left( -\frac{V_{11}}{\hbar} + \omega_0 \right) \right] - 2\gamma \right\} \tilde{\rho}_{ccvv} \\ & - 0.5i\Omega^*(t) (2\tilde{\rho}_{ccvc} + 2\tilde{\rho}_{ccvc}^* - \tilde{\rho}_{vc,2}^* - \tilde{\rho}_{vc,1}^*), \end{aligned} \quad (33)$$

with the Rabi frequency  $\Omega^* = \frac{\tilde{\mathbf{E}}(t) \cdot \mathbf{d}_{cv}}{\hbar} e^{i(\omega_L - \omega_0)t}$ . The damping constant  $\gamma$  results from the Markovian fully quantized electron-light interaction and is given by  $\gamma = \pi \frac{G_{cv}^2}{\hbar^2} n_{\text{ph}}$ , where  $n_{\text{ph}}$  is the density of phonon states. For the numerical calculations the RWA frequency  $\omega_0$  is set to  $\omega_1$ .

### VIII. RESULTS: OPTICAL PROPERTIES

An ensemble of semiconductor quantum dots shows a distribution in size and therefore resonance energies that depend on the material and the manufacturing process. Regarding the optical properties of two adjacent quantum dots during laser excitation, the resonance energy difference is an important quantity. Selective excitation of the dots, for example, is very difficult to obtain for quantum dots with small energy difference. To emphasize the effect of the resonance energy difference, we contrast two situations: first, a system of two quantum dots with a difference in resonance energies of  $\Delta = 10$  meV. That difference allows a spectrally selective exci-

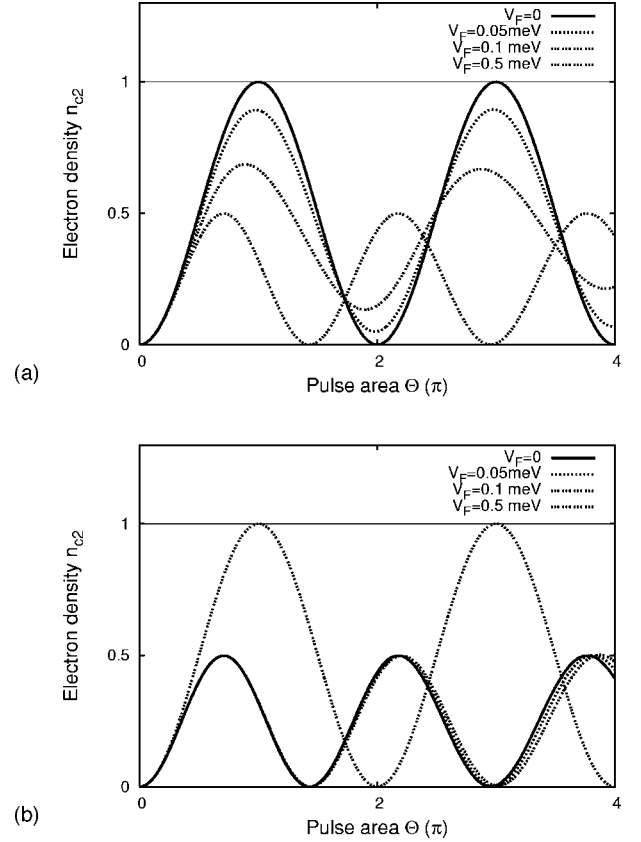


FIG. 8. Rabi oscillation of the upper electron density with and without Förster coupling for identical quantum dots. The pulse is resonant to the higher-energy resonance. Top: vanishing biexcitonic shift. Bottom: strong biexcitonic shift ( $V_{11} = 1$  meV).

tation of the single dots with picosecond pulses as utilized in most of the situations investigated here. Second, we compare the nonidentical dots to a system of two identical quantum dots to understand an idealized theoretical model system.

The radiative single-dot damping constant used for calculating the linear and nonlinear optical spectra is taken to be  $\gamma = (500 \text{ ps})^{-1}$ , as measured in low-temperature experiments.<sup>8</sup>

Depending on various parameters, the Coulomb matrix elements have been shown to reach values of up to a few meV for the biexcitonic shift and the Förster matrix element.<sup>6,12</sup> Since we want to investigate the general effects of the Coulomb coupling instead of describing a special quantum dot structure, we mostly show results for this highest range of realistic values of the matrix elements to emphasize the effect of Coulomb interaction here.

#### A. Linear optics: Absorption spectra

We first investigate the (spectral) properties of the system under the influence of a weak laser pulse by calculating linear absorption spectra. In linear optics, the biexcitonic contribution  $V_{11}$  that shifts the resonance energy of the biexcitonic transition cannot be observed since it is a nonlinear effect and therefore will not be considered in this section. In contrast to that, the Förster coupling leads to new resonance energies of the single-excitonic transitions being observable

in linear optics. So one expects to observe a line shift in the linear absorption spectra depending on the Förster matrix element  $V_F$ .

*Nonidentical quantum dots* ( $\Delta=10$  meV). For different quantum dots energies the upper resonance energy increases while the lower decreases with rising  $V_F$ , respectively. Figure 1 shows the linear absorption spectra for different values of  $V_F$  for the coupled quantum dot resonances. The spectra are plotted versus detuning of the uncoupled lower quantum dot resonance. As can be seen, an energy shift  $\delta$  occurs that depends on  $V_F$  and is smaller than the value of the matrix element. Following Eq. (17), this shift is given by  $\delta=\frac{1}{2}(\Delta-\sqrt{\Delta^2-4V_F^2})$ . The shifted positions of the absorption lines that result from this formula are plotted in the figure as vertical lines.

As expected, its value is the same for both quantum dot resonances, however the sign is different.

*Identical quantum dots* ( $\Delta=0$ ). For identical quantum dots the situation is different: from the discussion in Sec. IV it follows that only one resonance can be excited optically and therefore only one absorption line occurs in the spectrum. In this case the transition energy simplifies to  $\hbar\omega_1+|V_F|$ , so the shift is directly given by the value of the matrix element. The corresponding absorption spectra can be seen in Fig. 2.

Comparing the two cases of different and identical quantum dots, it can be recognized that the shift of the absorption lines has the size of the Förster matrix element for identical quantum dots while the shift is smaller when a difference in the resonance energies of the dots occurs: therefore, the relative influence of the Förster coupling on the spectral properties becomes stronger for decreasing energy differences. Furthermore, the lower absorption line gets weaker with decreasing energy difference, leaving only one optically excitable transition for coupled identical quantum dots.

### B. Single-pulse excitation

Now we discuss the behavior of the system under the influence of a strong coherent light pulse, thus entering the nonlinear optical regime where a significant electron occupation in the upper level is built up. The spectrally narrow pulse (5-ps pulse) is taken to be resonant to one of the single-exciton resonances; the second resonance has a negligible spectral overlap with the pulse spectrum. The pulse area is defined by  $\Theta=\int_{-\infty}^{\infty} dt \tilde{\Omega}(t)$ .

To emphasize the effect of the interplay between electron-light interaction and Coulomb coupling between the dots we can safely ignore the radiative damping in this section, since it contributes only on longer time scales than depicted here.

*Nonidentical quantum dots.* The resonance energy difference in the presence of Förster coupling is given by  $\sqrt{\Delta^2+4V_F^2}$ . In the case considered here ( $\Delta=10$  meV), the use of temporally long and spectrally narrow pulses with a temporal width in the range of a few ps allows for selective excitation of single, well-isolated resonances as occurring in the linear optical spectra. The creation of biexcitons (transition to  $|\psi_4\rangle$ ) in the two-dot system can thus be excluded for sufficiently spectrally narrow single-pulse excitation. As a consequence the biexcitonic shift has no influence on the

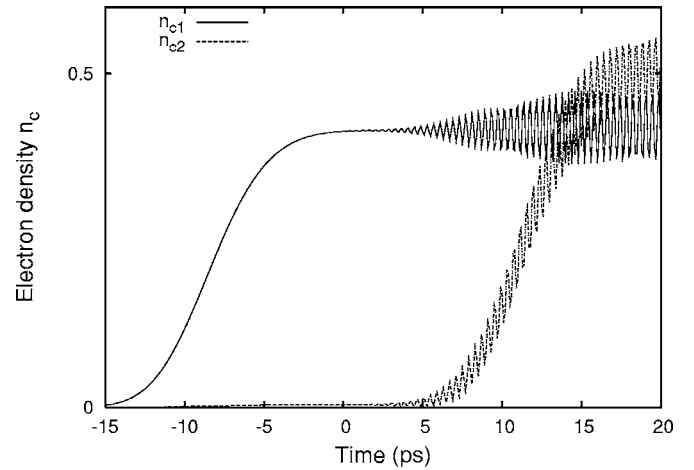


FIG. 9. Temporal evolution of the electron densities for two-pulse excitation with 5-ps pulses with a pulse area of  $\pi/2$  and a pulse delay of 20 ps. The Förster matrix element is taken to be  $V_F=1$  meV.

processes considered here [cf. Eq. (17)]. For the following calculations we therefore assume a biexcitonic shift of  $V_{11}=0$  and investigate the influence of the Förster coupling on single-pulse excitations.

We now investigate the case in which one of the two resonances of the system is resonantly excited. The temporal behavior of the electron density and polarization in the individual dots is discussed for excitation of the lower as well as the higher resonance of the coupled system.

Figure 3 shows density and polarization of both quantum dots during excitation with a 5-ps pulse with pulse area  $\pi$  for different values of the Förster matrix element. Here, the pulse is resonant to the lower resonance energy, while in Fig. 4 the same is shown for resonant excitation of the higher resonance. For resonant excitation of the lower resonance (Fig. 3) the density and polarization of the lower-energy quantum dot (left column) do not reach the final values of the uncoupled system, which would be full inversion of the electron density and zero polarization. Furthermore, the higher-resonance quantum dot reacts to the pulse as well, which is not the case in the uncoupled system. When the higher resonance is resonantly excited (Fig. 4), it can be seen that the density in this case passes a maximum and the absolute value of the polarization reaches zero once, but rises to a nonzero value afterwards. This difference results from the renormalization of the Rabi frequency due to Förster coupling [see Eq. (21) on the lower-energy resonance the  $\pi$  pulse acts as a pulse with a diminished pulse area while for the higher resonance it acts as a pulse of a higher pulse area]. Therefore the dynamic quantities of the lower resonance do not reach the final values corresponding to a that of a  $\pi$  pulse but the quantities of the higher resonance pass them (a maximum of the density and a zero of the polarization).

Due to the formation of the new basis states in the coupled case, the coherent pulse causes a transition between the ground state and one of the new basis states  $|\Psi_2\rangle=(c_1|01\rangle+c_2|10\rangle)$ ,  $|\Psi_3\rangle=(-c_2|01\rangle+c_1|10\rangle)$ , which are superpositions of excited electron states in both dots. Since neither of the two coefficients is zero for nonvanishing  $V_F$ ,

the upper-state electron density in a single dot cannot reach the value of 1 anymore, even if only one of these resonances is excited.

In particular, the formation of the new states implies that as soon as there is Förster coupling in the system, it is not possible to excite an electron localized in a single quantum dot anymore using one resonant pulse (which is assumed to be a plane wave and has no spatial selectivity to excite a single dot). This can be seen in Figs. 3 and 4 from the fact that in each of the situations the density matrix elements of both dots react to the pulse. To explicate this effect we have plotted the electron densities of both dots in Fig. 5 for excitation resonant to the higher-energy transition. The exciting pulse is a  $\pi$  pulse with a width of 5 ps. In the inset the electron density of the second dot and the sum of both densities are shown around the maximum. The Förster coupling is taken to be 1 meV in order to stress the effect of the coupling, and the curve of the lower density is multiplied by a factor of 10 for visibility. As one can see, the electron densities of both dots are excited. The normalization of the state can be seen in the inset of Fig. 5 from the fact that the sum of the densities reaches the value of 1.

*Identical quantum dots.* In this case the dynamics is of increased complexity. Though there is only one single-exciton resonance that can be optically excited, due to the small energy difference of the resonances, the biexcitonic shift now plays a major role in the temporal dynamics: since the single-exciton resonance energy in that case is given by  $\hbar\omega_1 + |V_F|$  and the transition energy from the single-exciton to the biexciton state is given by  $\hbar\omega_1 - |V_F| + V_{11}$ , their energy difference is given by the Coulomb matrix element as  $V_{11} - 2|V_F|$  (see Appendix A). Whether or not the single-excitonic resonances can be selectively excited spectrally without excitation of the biexciton depends on the size of both matrix elements. For small values (weak interaction) of the coupling matrix elements a single pulse can simultaneously excite the single exciton as well as the biexciton, for large values (strong interaction) selective excitation is possible.

These two cases show a different time behavior; cf. Fig. 6. If only the single-exciton resonance is excited (strong interaction, large biexciton energy), the final values of the density matrix elements are temporally constant after the pulse, similar to the situation of different quantum dots. In Fig. 6 (left) this can be seen for  $V_F = 0.1$  meV and  $V_{11} = 5$  meV and excitation with a 5-ps  $\pi$  pulse. The maximum value of the excited electron density in this case is 0.5, since the single-exciton states for identical quantum dots represent an equal superposition of the excitation in each of the two dots [see Eq. (23)]. Due to the renormalization of the Rabi frequency (for identical quantum dots the Rabi frequency for the single-exciton resonance gets multiplied by a factor  $\sqrt{2}$ ), the electron density passes its maximum for excitation with a  $\pi$  pulse.

The situation changes drastically when the biexcitonic shift vanishes (representing an extreme weak Coulomb coupling,  $V_{11} = 0$ ). Then the pulse creates a superposition of the single-exciton and biexciton states leading to oscillations of the absolute value of the polarization (see Appendix A). This is plotted in Fig. 6 (right). The polarization oscillates with a

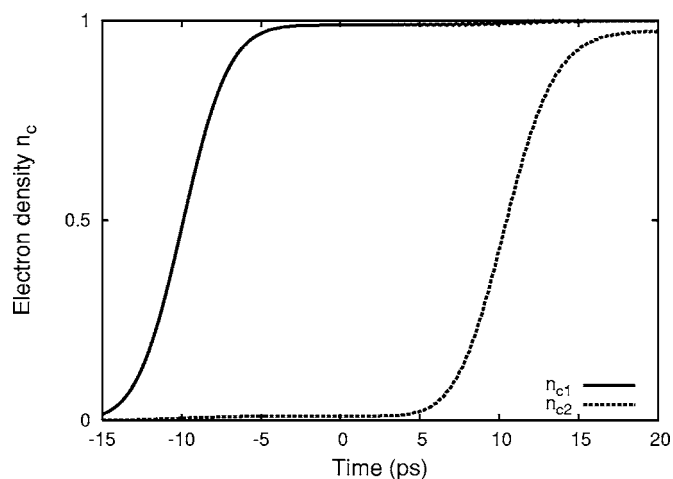


FIG. 10. Temporal evolution of the electron densities for two-pulse excitation with 5-ps pulses with a pulse area of  $\pi$  (renormalized for the first pulse according to  $V_F$ ) and a pulse delay of 20 ps. The Förster matrix element is taken to be  $V_F = 1$  meV.

frequency determined by  $V_F$  (see Appendix A).

The difference in the time behavior between identical and nonidentical quantum dots is of special importance for possible applications in quantum information theory: in quantum information applications one has to be able to selectively address the single qubits and prepare them in quantum mechanical states that change only when quantum operations are performed. Furthermore, there has to be an interaction mechanism between the qubits that allows the implementation of conditional operations. The Coulomb interaction is one promising candidate for the implementation of conditional operations.<sup>12</sup> Nevertheless, from our results we see that it also effects the possibility to selectively excite the excitonic resonances that would constitute the qubit states. The Förster interaction not only mixes the states but also causes oscillations of the density matrix elements in the case of identical quantum dots. Thus, for successful quantum information processing in a two-quantum-dot system one must be able to carefully control both parts of the Coulomb interaction and to select quantum dot pairs, whose resonance energy difference allows for selective excitation.

### 1. Rabi oscillations

In contrast to the last section where we investigated the time behavior during  $\pi$ -pulse excitation we now focus on the dynamics as a function of the pulse area, especially on the final state of the system. When the pulse area  $\Theta$  is varied for single-pulse excitation, Rabi oscillations are observed; i.e., the final value of the electron density after optical excitation oscillates as a function of the pulse area.<sup>13</sup>

*Nonidentical quantum dots.* First we discuss the case in which the different resonances are selectively excited by spectrally narrow pulses (again,  $V_{11} = 0$ ). We plot the final values of the electron density versus the pulse area for both quantum dots with and without Förster coupling in Fig. 7. Again, two situations are shown: the lower-energy resonance is excited (top row) and the higher-energy resonance is excited (bottom row). The strength of the coupling is set to the

high value of  $V_F=1$  meV to allow for a clear distinction of the curves in the plots. The effect of the Coulomb coupling on the Rabi oscillations is twofold: first, the amplitude of the oscillations decreases in the presence of coupling, and second, the oscillation period changes.

In Fig. 7 one can see that the amplitude of the oscillations decreases for both quantum dots in the coupled case. The oscillation amplitude is then expected to reduce to  $|c_1|^2$ , which depends on  $V_F$  [compare Eq. (18)].

The change in the oscillation period, however, is different for the two resonances: for the lower-energy resonance the oscillation period increases (Fig. 7, top row), while for one with the higher resonance energy the period decreases (Fig. 7, bottom row). This is again due to the different renormalization of the Rabi frequency; cf. Eq. (20). Accordingly, for a given pulse area of  $\pi$ , the density on the first dot has not yet reached its maximum, whereas the density in the second dot has already passed through its maximal value as seen in Figs. 5 and 6 for the case of a  $\pi$  pulse.

*Identical quantum dots.* The behavior for identical quantum dots regarding the occurrence of Rabi oscillations depends strongly on the possibility to selectively excite the single-excitonic and biexcitonic resonances.

When the biexcitonic shift is small, the possibility to selectively excite the resonances depends on the magnitude of  $V_F$ : in Fig. 8 (top) Rabi oscillations of the upper electron density are shown for  $V_{11}=0$  and varying  $V_F$  for excitation with a 5-ps pulse. For  $V_F=1$  meV the density oscillates between zero and 0.5 representing the case where only the single-excitonic transition is excited since an energy difference of 1 meV allows for selective excitation. With decreasing  $V_F$  the maximal value of the density rises, since the biexcitonic transition gets more and more excited. For small values of  $V_F$  the maximum converges to 1, leading to the uncoupled case, where both the single-exciton and biexcitonic transitions are excited.

When the same situation is calculated for a biexcitonic shift of  $V_{11}=1$  meV, the energy difference between the single-excitonic and biexcitonic transition is big enough to allow for selective excitation even for small values of the Förster matrix element. Therefore one expects the electron density to oscillate between zero and 0.5 for a wide range of the Förster coupling. This can be seen in Fig. 8 (bottom). The oscillation period then decreases to  $\sqrt{2}$ , as expected from the analytical discussion [cf. Eq. (22)]. Only if the energy shift due to Förster coupling reaches the size of the biexcitonic shift, the single-excitonic and biexcitonic resonance can be excited simultaneously again, which is the case for  $V_F=1/2V_{11}$ . Then, again, the electron density reaches the value of 1.

One has to stress here that as soon as there is Coulomb coupling in the system of two identical quantum dots, the only way to reach an electron density of 1 in one of the quantum dots is to simultaneously excite the single-excitonic and the biexcitonic resonance (as long as the quantum dots cannot be spatially selectively excited). In terms of quantum information this implies that qubits represented by excitons in the single dots cannot be manipulated sufficiently. Therefore a resonance energy of the quantum dots that allows for selective excitation of the single-excitonic resonances is of

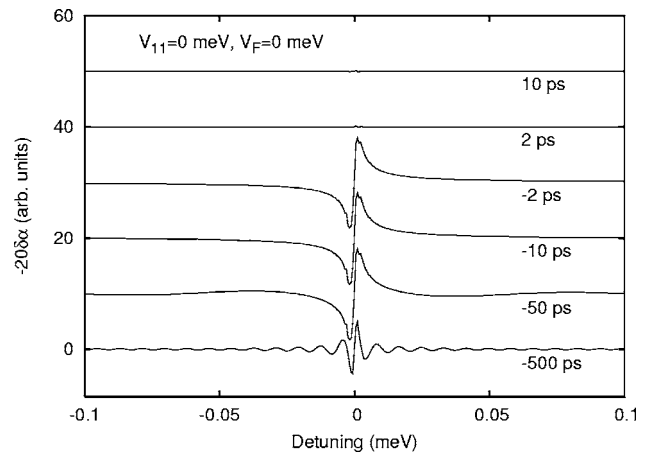


FIG. 11. Differential transmission spectra (DTS) for a system of two uncoupled quantum dots for different time delays. The radiative damping is  $\gamma=(500 \text{ ps})^{-1}$ . The probe pulse excites the higher-energy resonance; shown is the energy region around the lower-energy resonance.

vital importance for quantum information applications of such a system.

## 2. Two-pulse excitation

For optical implementations of quantum information processing the behavior of a qubit system under more complex situations than single-pulse excitation is essential to know. Complex operations on qubits would be implemented by applying a number of pulses with differing resonance energies, pulse areas, and pulse lengths. For example, the implementation of the CNOT operation in Ref. 12 involves a series of two pulses. As a next step we therefore investigate the effects of the Coulomb interaction occurring during two-pulse excitation of the system.

In this subsection we describe the following situation: the system is excited by two spectrally narrow light pulses, each of them being resonant to one of the two single-excitonic resonances. Since only one of the resonances can be excited for identical quantum dots, we only describe the case of different quantum dots here. In two-pulse excitation the driving light field not only causes transitions between the ground state and one of the excited states but between the ground and two excited states. As a result the state of the system can be a superposition of three states of different energies, depending on the pulse area of the two exciting pulses, leading to new effects in the time behavior of the system. Analogous to the case of single-pulse excitation of identical quantum dots, oscillations of the density matrix elements occur.

In Fig. 9 the two upper electron densities of the two quantum dots are shown for excitation with two pulses, each having a pulse area of  $\Theta=0.5\pi$ . The pulses have a temporal width of 5 ps, and the time delay between the pulses is 20 ps. Again the biexcitonic shift is set to zero. Starting with the second pulse, both electron densities start oscillations that continue after the second pulse ended. The densities oscillate in antiphase, so the sum of the densities is constant. The oscillations arise from the fact that each pulse creates an

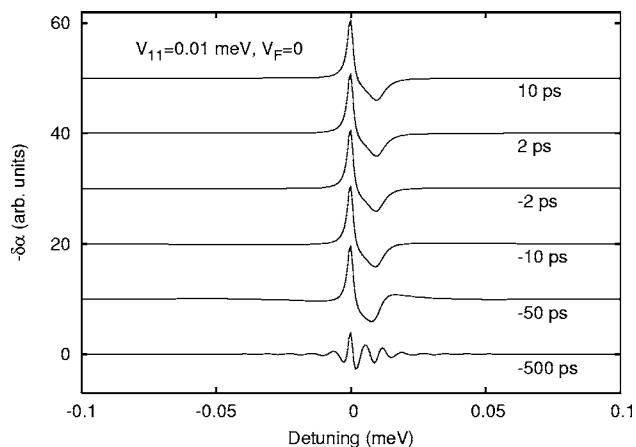


FIG. 12. DTS for two quantum dots coupled by the diagonal Coulomb interaction for different time delays: the biexcitonic shift results from the matrix element  $V_{11}=0.01$  meV.

equal superposition of the ground and the respective excited state. Therefore, after the second pulse the state resembles a superposition of the ground and two excited states. Since both excited states contain an upper electron state in each dot, but with different energies, the electron density in each dot starts to oscillate.

Since the oscillations depend on the creation of a superposition of the two excited states, they vanish if the state created by the series of pulses does not contain both excited states. This is the case if the pulses do not create a superposition—for example, when both pulse areas have the value  $\Theta = \pi$  (renormalized for the first pulse according to the value of  $V_F$ ). Then the first pulse changes the state from  $|\Psi_0\rangle$  to  $|\Psi_1\rangle$  and the second pulse changes the state from  $|\Psi_1\rangle$  to  $|\Psi_3\rangle$ . This situation is shown in Fig. 10: the resulting densities do not oscillate.

### IX. DIFFERENTIAL TRANSMISSION SPECTRA

The analysis of differential transmission spectra (DTS) is one way to obtain information about the Coulomb coupling parameters from experiment.<sup>16</sup> Here, we describe the following experimental situation: The quantum dot sample is excited with a pump pulse of area  $\Theta = \pi$  and a small spectral linewidth, which is resonant to the higher resonance of the coupled system. This results in the formation of an exciton in the resonantly excited state, which then decays due to radiative damping. Transmission spectra of a spectrally broad probe pulse with a small pulse area ( $\Theta = 0.01\pi$ ) are taken with varying time delay relative to the pump pulse. It has to be emphasized here that in the presence of Coulomb coupling the pulse area has to be renormalized to achieve the desired excitation, since the excitation applies for new eigenstates. This is in accordance with the experimental situation, where one would define a  $\pi$  pulse by the resulting maximum electron density.

Differential transmission spectra represent the difference of the probe spectra with and without the pump pulse.<sup>2,23</sup> The DTS can be calculated as follows:

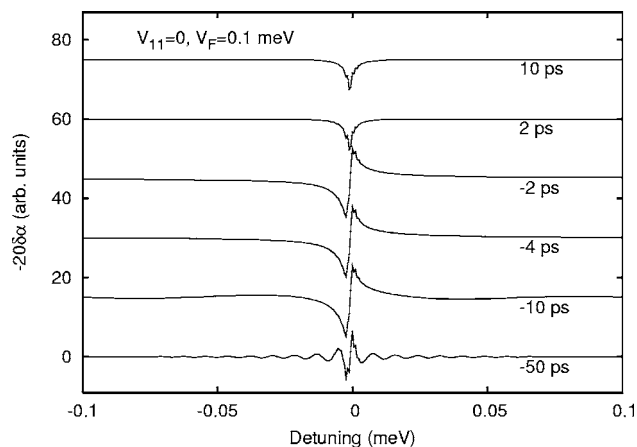


FIG. 13. DTS for two quantum dots coupled by the nondiagonal Coulomb interaction for different time delays: the Förster matrix element  $V_F$  has a value of  $V_F=0.1$  meV.

$$\text{DTS}(\omega) = \frac{T(\omega) - T_0(\omega)}{T_0(\omega)} \propto -\delta\alpha(\omega) = \alpha_0(\omega) - \alpha(\omega), \quad (34)$$

where  $\alpha_0(\omega)$  and  $\alpha(\omega)$  denote the probe absorption without and with the pump laser. The differential transmission spectra are calculated using the following parameters: resonance energy difference of the two quantum dots,  $\Delta = 10$  meV; radiative damping constant  $\gamma = 1/500$  ps; temporal widths of the pump pulse and probe pulse, 2 ps and 100 fs, with pulse areas of  $\Theta = \pi$  and  $\Theta = 0.01\pi$ , respectively. Positive time delay denotes the probe following the pump pulse. The plotted spectra show the differential transmission of the nonresonant quantum dot versus the detuning to the uncoupled resonance for different time delays between pump and probe pulse. Since the probe pulse is spectrally broad, it can excite all resonances of the coupled system. Especially the biexcitonic transition can be excited if a single exciton has been created by the pump pulse. Therefore this method provides information about both parts of the Coulomb coupling.

Without a Coulomb interaction (see Fig. 11) the nonlinear optical Stark effect causes oscillations for negative time delay and a dispersive line shape for small delay times,<sup>23</sup> also for single quantum dots.<sup>24</sup> This dispersive line shape represents the spectral shift of the two Coulomb interaction mechanisms, however, have different effects on the spectra: First of all, they are internal fields and cause a contribution long after the action of the pump pulse—i.e., at positive time delays. The biexcitonic shift causes an energy shift which results in a dispersive line shape. Since the shift is an intrinsic property of the coupled dot system [cf. Eq. (17)], it does not depend on an interaction of pump and probe pulse. Therefore it can be observed for either positive and negative time delay, as seen in Fig. 12 for a biexcitonic shift  $V_{11} = 0.1$  meV. Depending on the magnitude and sign of the biexcitonic shift it can cancel the effect of the optical Stark effect, as observed in recent experiments.<sup>16</sup> This is the case in Fig. 12: the dispersive line shape is reversed compared to Fig. 11.

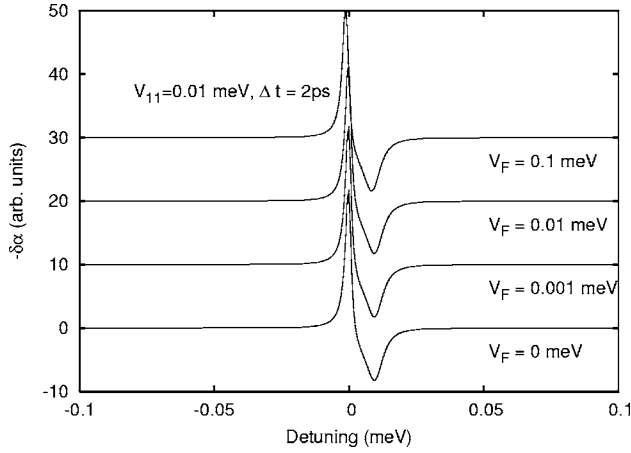


FIG. 14. DTS for two quantum dots for a biexcitonic shift of  $V_{11}=0.01$  meV and different values of the Förster matrix element. The spectra are shown for fixed time delay of  $\Delta t=2$  ps.

The impact of the Förster effect on the DTS is completely different, which can be seen in Fig. 13. Here the DTS are shown for  $V_F=0.1$  meV. Although Förster coupling also causes a line shift, this shift does not depend on the presence of the pump pulse. Therefore there is no resulting dispersive line shape in the DTS. Due to the resulting energy transfer, it rather leads to an absorptive line shape at the shifted resonance. This can also be seen from the analytical discussion (see Appendix A).

It has to be stressed that the Förster effect results in much weaker signatures in the DTS compared to the biexcitonic shift, especially with respect to the magnitude of the matrix elements. To show this we plot the DTS for a fixed time delay of  $\Delta t=+2$  ps (Fig. 14). The biexcitonic shift is taken to be 0.01 meV, and the Förster effect varies between 0.0 and 0.1 meV. Even for  $V_F=0.1$  meV, where the Förster matrix element is one order of magnitude larger than the biexcitonic shift, the line shape is not strongly modified. Even the line shift of 0.001 meV caused by  $V_F=0.1$  meV is only barely noticeable, since it is too small. As a consequence it is much more difficult to obtain information about the Förster matrix element from differential transmission spectra than about the biexcitonic shift.

## X. CONCLUSIONS

We have shown that the Förster coupling affects single-pulse excitation of coupled quantum dots and Rabi oscillations in two ways: the maximum value of the single-electron densities decreases due to Förster coupling and the period of the Rabi oscillations is renormalized. For different quantum dots the period of the lower-energy resonance increases; the one of the higher resonance decreases with rising strength of the Förster coupling. The amplitude is always diminished. For identical quantum dots only one resonance can be optically excited in the presence of Förster coupling, with decreased amplitude and period of the Rabi oscillations. Both effects are of special importance for quantum information applications, since they influence the possibility to coher-

ently control qubits in quantum dot systems by optical means. We have also discussed the temporal dynamics of the system during pulsed excitation; the development of the system in time depends sensitively on the relative magnitudes of the coupling parameters, the differences in resonance energies of the two dots, and the spectral width of the pulses.

The discussion of qualitative and quantitative influences of Coulomb coupling on differential transmission spectra confirms recent experimental results obtained by Unold *et al.*<sup>16</sup> Nevertheless, we have shown that the Förster coupling causes much weaker signatures in these experiments than the biexcitonic shift. Therefore it seems advisable to use other experimental techniques to determine the strength of the Förster coupling in quantum dot systems.

Typically the restriction to a two-level system and one fixed polarization (either circular or linear) fails if the fine-structure splitting is in the same order in comparison to the interaction energy like Förster or biexciton contributions. In this sense, our system must be regarded as a first model approach and the Förster and biexciton coupling strength was arbitrarily chosen to illustrate basic effects.

## ACKNOWLEDGMENTS

J. D. thanks Lukas Novotny for support, helpful discussions, and hospitality in Rochester. We thank C. Lienau (MBI Berlin) for discussions and the DFG for support through Grant No. Sfb 296 (Wachstumskorrelierte Eigenschaften niederdimensionaler Halbleiterstrukturen).

## APPENDIX A: TEMPORAL EVOLUTION OF STATES FOR IDENTICAL QUANTUM DOTS DURING SINGLE-PULSE EXCITATION

If the two Coulomb-coupled quantum dots are identical ( $\omega_1=\omega_2$ ), the system of basis states and eigenenergies has the form

$$|\Psi_1\rangle = |00\rangle, \quad \lambda_1 = \hbar \omega_0 + V_{00},$$

$$|\Psi_2\rangle = \frac{1}{\sqrt{2}}(-|01\rangle + |10\rangle), \quad \lambda_3 = \hbar \omega_0 + \hbar \omega_1 - |V_F| + V_{01},$$

$$|\Psi_3\rangle = \frac{1}{\sqrt{2}}(|01\rangle + |10\rangle), \quad \lambda_2 = \hbar \omega_0 + \hbar \omega_1 + |V_F| + V_{01},$$

$$|\Psi_4\rangle = |11\rangle, \quad \lambda_4 = \hbar \omega_0 + 2 \hbar \omega_1 + V_{11}. \quad (\text{A1})$$

To emphasize the effect of the Förster matrix element on the temporal evolution we neglect the diagonal terms  $V_{00}$  and  $V_{01}$  in the following discussion. The resonance energies for the creation of a single exciton are the given by

$$|\Psi_1\rangle \rightarrow |\Psi_3\rangle: \Delta E_{13} = \hbar \omega_1 + |V_F|,$$

$$|\Psi_1\rangle \rightarrow |\Psi_2\rangle: \Delta E_{12} = \hbar \omega_1 - |V_F| \quad (\text{A2})$$

and the resonance energies for the creation of a biexciton by

$$|\Psi_3\rangle \rightarrow |\Psi_4\rangle: \Delta E_{34} = \hbar \omega_1 - |V_F| + V_{11},$$

$$|\Psi_2\rangle \rightarrow |\Psi_4\rangle: \Delta E_{24} = \hbar \omega_1 + |V_F| + V_{11}. \quad (\text{A3})$$

Depending on the size of the coupling matrix elements and the pulse width there are different possible regimes for the excitation of the system (which is initially in the ground state  $|\Psi_1\rangle$ ) with one coherent laser pulse. In the following these regimes are compared for excitation with a pulse that creates an equal superposition of the ground and excited states (in the uncoupled system this would be achieved with a pulse of pulse area  $\Theta = \frac{\pi}{2}$ ; in the presence of Coulomb coupling, the area has to be renormalized):

(i) Both Coulomb matrix elements are big enough to allow for selective excitation: then, the pulse creates a superposition of the ground and resonant excited states (for example,  $|\Psi_3\rangle$ ). The created state will have the form

$$\begin{aligned} |\Psi\rangle &= \frac{1}{\sqrt{2}}(|00\rangle - i|\Psi_3\rangle) = \frac{1}{\sqrt{2}}\left(|00\rangle - i\frac{1}{\sqrt{2}}(|01\rangle + |10\rangle)\right) \\ \rightarrow |\Psi(t)\rangle &= \frac{1}{\sqrt{2}}\left(|00\rangle e^{i\omega_0 t} - i\frac{1}{\sqrt{2}}(|01\rangle + |10\rangle) e^{i(\omega_0 + \omega_1 + |V_F|/\hbar)t}\right). \end{aligned} \quad (\text{A4})$$

The corresponding density matrix is given by

$$\begin{aligned} \hat{\rho}_{|\Psi(t)\rangle} &= \frac{1}{2}\left[|00\rangle\langle 00| - \frac{i}{\sqrt{2}}(|10\rangle\langle 00| + |01\rangle\langle 00|) e^{i(\omega_1 + |V_F|/\hbar)t} \right. \\ &\quad - (|00\rangle\langle 10| + |00\rangle\langle 01|) e^{-i(\omega_1 + |V_F|/\hbar)t} + \frac{1}{2}(|01\rangle\langle 01| \\ &\quad \left. + |10\rangle\langle 10| + |01\rangle\langle 10| + |10\rangle\langle 01|)\right]. \end{aligned} \quad (\text{A5})$$

The reduced density matrices of the individual quantum dot electrons are then given by

$$\begin{aligned} \text{Tr}(\hat{\rho}_{|\Psi(t)\rangle})_2 &= \frac{3}{4}|0\rangle\langle 0| - \frac{i}{\sqrt{2}}|1\rangle\langle 0| e^{i(\omega_1 + |V_F|/\hbar)t} + \frac{i}{\sqrt{2}}|0\rangle \\ &\quad \times \langle 1| e^{-i(\omega_1 + |V_F|/\hbar)t} + \frac{1}{4}|1\rangle\langle 1|, \\ \text{Tr}(\hat{\rho}_{|\Psi(t)\rangle})_1 &= \frac{3}{4}|0\rangle\langle 0| - \frac{i}{\sqrt{2}}|1\rangle\langle 0| e^{i(\omega_1 + |V_F|/\hbar)t} + \frac{i}{\sqrt{2}}|0\rangle \\ &\quad \times \langle 1| e^{-i(\omega_1 + |V_F|/\hbar)t} + \frac{1}{4}|1\rangle\langle 1|. \end{aligned} \quad (\text{A6})$$

As one can see, the nondiagonal terms representing the polarizations show a time dependence of  $e^{i(\omega_1 + |V_F|/\hbar)t}$ . Therefore, in this case the absolute value of the individual polarizations shows no time dependence. The diagonal terms representing the single-electron densities show no time dependence at all.

(ii) Small  $V_F$ , small  $V_{11}$ : the single-excitonic resonance cannot be excited selectively from the biexcitonic resonance. In this case the  $\frac{\pi}{2}$  pulse can excite the single-excitonic transition  $|00\rangle \rightarrow |\Psi_3\rangle$  and the biexcitonic transition  $|\Psi_3\rangle \rightarrow |\Psi_4\rangle$ , simultaneously. The created state has the form

$$\begin{aligned} |\Psi\rangle &= \frac{1}{\sqrt{2}}\left(|00\rangle - \frac{i}{\sqrt{2}}(|\Psi_3\rangle - i|\Psi_4\rangle)\right) \\ &= \frac{1}{\sqrt{2}}\left[|00\rangle - \frac{i}{\sqrt{2}}\left(\frac{1}{\sqrt{2}}(|01\rangle + |10\rangle) - i|11\rangle\right)\right] \\ \rightarrow |\Psi(t)\rangle &= \frac{1}{\sqrt{2}}\left[|00\rangle e^{i\omega_0 t} - \frac{i}{\sqrt{2}}\left(\frac{1}{\sqrt{2}}(|01\rangle + |10\rangle) e^{i(\omega_0 + \omega_1 + |V_F|/\hbar)t} \right. \right. \\ &\quad \left. \left. - i|11\rangle e^{i(\omega_0 + 2\omega_1 + 2V_{11}/\hbar)t}\right)\right]. \end{aligned} \quad (\text{A7})$$

The corresponding density matrix then reads as

$$\begin{aligned} \hat{\rho}_{|\Psi(t)\rangle} &= \frac{1}{2}\left[|00\rangle\langle 00| - \frac{i}{2}[(|10\rangle\langle 00| + |01\rangle\langle 00|) e^{i(\omega_1 + |V_F|/\hbar)t} \right. \\ &\quad \left. - (|00\rangle\langle 10| + |00\rangle\langle 01|) e^{-i(2\omega_1 + |V_F|/\hbar)t}] \right. \\ &\quad \left. - \frac{1}{\sqrt{2}}(|00\rangle\langle 11| e^{-i(\omega_1 + V_{11}/\hbar)t} - |11\rangle\langle 00| e^{-i(\omega_1 + V_{11}/\hbar)t}) \right. \\ &\quad \left. + \frac{1}{4}(|01\rangle\langle 01| + |10\rangle\langle 10| - |01\rangle\langle 10| - |10\rangle\langle 01|) \right. \\ &\quad \left. + \frac{i}{2\sqrt{2}}[(|01\rangle\langle 11| + |10\rangle\langle 11|) e^{-i(\omega_1 - 2|V_F|/\hbar + V_{11}/\hbar)t} \right. \\ &\quad \left. - (|11\rangle\langle 01| + |11\rangle\langle 10|) e^{i(\omega_1 - 2|V_F|/\hbar + V_{11}/\hbar)t}] \right. \\ &\quad \left. + \frac{1}{2}|11\rangle\langle 11|\right], \end{aligned} \quad (\text{A8})$$

and the reduced density matrices follow as

$$\begin{aligned} \text{Tr}(\hat{\rho}_{|\Psi(t)\rangle})_2 &= \frac{3}{4}|0\rangle\langle 0| - \left(\frac{i}{4} e^{i(\omega_1 + |V_F|/\hbar)t} + \frac{i}{4\sqrt{2}} e^{i(\omega_1 - |V_F|/\hbar + V_{11}/\hbar)t}\right) \\ &\quad \times |1\rangle\langle 0| + \left(\frac{i}{4} e^{-i(\omega_1 + |V_F|/\hbar)t} \right. \\ &\quad \left. + \frac{i}{4\sqrt{2}} e^{-i(\omega_1 - |V_F|/\hbar + \frac{V_{11}}{\hbar})t}\right) |0\rangle\langle 1| + \frac{1}{4}|1\rangle\langle 1| \\ \text{Tr}(\hat{\rho}_{|\Psi(t)\rangle})_1 &= \frac{3}{4}|0\rangle\langle 0| - \left(\frac{i}{4} e^{i(\omega_1 + |V_F|/\hbar)t} + \frac{i}{4\sqrt{2}} e^{i(\omega_1 - |V_F|/\hbar + V_{11}/\hbar)t}\right) \\ &\quad \times |1\rangle\langle 0| + \left(\frac{i}{4} e^{-i(\omega_1 + |V_F|/\hbar)t} \right. \\ &\quad \left. + \frac{i}{4\sqrt{2}} e^{-i(\omega_1 - |V_F|/\hbar + V_{11}/\hbar)t}\right) |0\rangle\langle 1| + \frac{1}{4}|1\rangle\langle 1|. \end{aligned} \quad (\text{A9})$$

Here, the diagonal parts show no time dependence. For the case of  $V_{11} = 0$  the nondiagonal parts have a time dependence of that is a sum of the two exponentials  $e^{i(\omega_1 + |V_F|/\hbar)t}$  and  $e^{i(\omega_1 - |V_F|/\hbar)t}$  with differing factors leading to an oscillation of the absolute value of the polarization with a frequency of  $\omega = \frac{|V_F|}{\hbar}$ . In contrast to that the electron densities show no time dependence in this case.

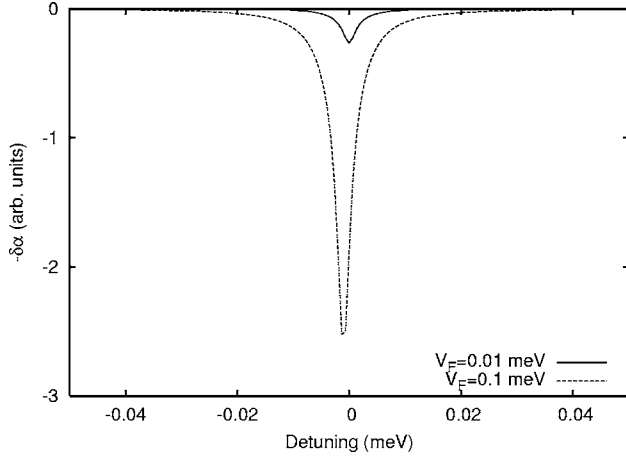


FIG. 15. DTS for two quantum dots for a biexcitonic shift of  $V_{11}=0$  meV and two different values of the Förster matrix element.

### APPENDIX B: ANALYTICAL CALCULATION OF DIFFERENTIAL TRANSMISSION SPECTRA

The system of equations of motion describing the pump and probe experiments can be solved analytically for positive time delays: we do this by assuming that the density matrix elements are weakly damped and can be taken as constant during excitation with short, weak probe pulses. Then the absorption spectrum of the probe pulse can be calculated using Fourier transformation for the system in the ground state as well as for the system that was excited by the strong pump pulses. The difference of these two spectra constitutes the differential transmission spectrum. We have to emphasize that the dynamic interaction between pump and probe pulse is not taken into account by this method.

Starting with the system of equations of motion we apply the Fourier transformation. Assuming that the exciting pulse can be described by a  $\delta$  function we get the following system of equations:

$$\begin{aligned}
 -i\omega\rho_{vc,1}(\omega) &= [-i(\omega_1 - \omega_0) - \gamma]\rho_{vc,1}(\omega) - \frac{i}{2\sqrt{2}}[n_{v,1}(0) \\
 &\quad - n_{c,1}(0)] + \left(\frac{iV_F}{\hbar}\right)[- \rho_{vc,2}(\omega) + 2\rho_{ccvc}^*(\omega)] \\
 &\quad - 2i\frac{V_{cc}}{\hbar}\rho_{ccvc}^*(\omega), \quad (B1)
 \end{aligned}$$

$$\begin{aligned}
 -i\omega\rho_{vc,2}(\omega) &= [-i(\omega_2 - \omega_0) - \gamma]\rho_{vc,2}(\omega) - \frac{i}{2\sqrt{2}}[n_{v,2}(0) \\
 &\quad - n_{c,2}(0)] + \left(\frac{iV_F}{\hbar}\right)[- \rho_{vc,1}(\omega) + 2\rho_{ccvc}^*(\omega)] \\
 &\quad - 2i\frac{V_{cc}}{\hbar}\rho_{ccvc}^*(\omega), \quad (B2)
 \end{aligned}$$

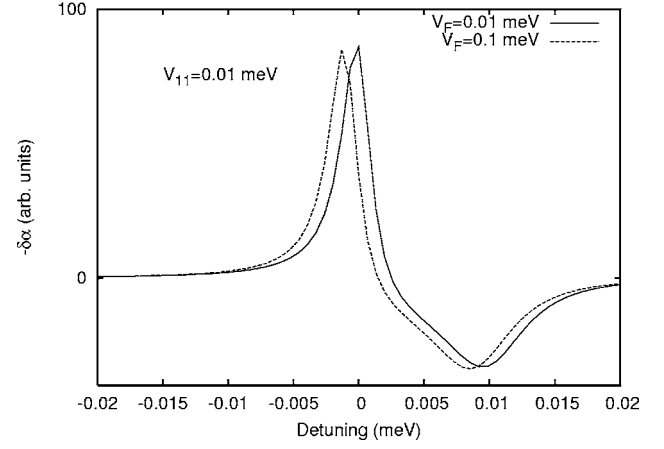


FIG. 16. DTS for two quantum dots for a biexcitonic shift of  $V_{11}=0.01$  meV and two different values of the Förster matrix element.

$$\begin{aligned}
 -i\omega n_{c,1}(\omega) &= \gamma[-n_{c,1}(\omega) - n_{c,1}^*(\omega)] - \frac{i}{2\sqrt{2}}[\rho_{vc,1}(0)^* \\
 &\quad - \rho_{vc,1}(0)] - \frac{iV_F}{\hbar}[\rho_{cvcv}(\omega) - \rho_{cvcv}^*(\omega)], \quad (B3)
 \end{aligned}$$

$$\begin{aligned}
 -i\omega n_{c,2}(\omega) &= \gamma[-n_{c,2}(\omega) - n_{c,2}^*(\omega)] - \frac{i}{2\sqrt{2}}[\rho_{vc,2}(0)^* \\
 &\quad - \rho_{vc,2}(0)] - \frac{iV_F}{\hbar}[\rho_{cvcv}^*(\omega) - \rho_{cvcv}(\omega)], \quad (B4)
 \end{aligned}$$

$$\begin{aligned}
 -i\omega\rho_{cccc}(\omega) &= -4\gamma_0\rho_{cccc}(\omega) - \frac{i}{2\sqrt{2}}\{[\rho_{ccvc}(0) + \rho_{cvcv}(0)] \\
 &\quad - [\rho_{ccvc}(0)^* + \rho_{cvcv}^*(0)]\}, \quad (B5)
 \end{aligned}$$

$$\begin{aligned}
 -i\omega\rho_{cvcv}(\omega) &= [-i(\omega_2 - \omega_1) - 2\gamma]\rho_{cvcv}(\omega) + \frac{i}{2\sqrt{2}}\{[\rho_{vc,2}(0) \\
 &\quad - 2\rho_{ccvc}^*(0)] + [-\rho_{vc,1}(0) + 2\rho_{ccvc}(0)]\} \\
 &\quad + \frac{iV_F}{\hbar}[-n_{c,1}(\omega) + n_{c,2}(\omega)], \quad (B6)
 \end{aligned}$$

$$\begin{aligned}
 -i\omega\rho_{cccv}(\omega) &= \left[-i\left(-\omega_1 + \omega_0 - 2\frac{V_{cc}}{\hbar}\right) - 3\gamma\right]\rho_{cccv}(\omega) \\
 &\quad + \frac{i}{2\sqrt{2}}\{[n_{c,2}(0) - 2\rho_{cccc}(0) + \rho_{cvcv}(0)] \\
 &\quad - \rho_{cvcv}(0)\} - \left(\frac{iV_F}{\hbar}\right)\rho_{ccvc}(\omega), \quad (B7)
 \end{aligned}$$

$$\begin{aligned}
-i\omega\rho_{ccvc}(\omega) = & \left[ -i\left(-\omega_2 + \omega_0 - 2\frac{V_{cc}}{\hbar}\right) - 3\gamma \right] \rho_{ccvc}(\omega) \\
& - \frac{i}{2\sqrt{2}}(\rho_{ccvv}(0) - \{\rho_{ccvv}(0)\}^*(0) + [n_{c,1}(0) \\
& - 2\rho_{ccc}(0)]) - \left(\frac{iV_F}{\hbar}\right)\rho_{cccv}(\omega), \quad (\text{B8})
\end{aligned}$$

$$\begin{aligned}
-i\omega\rho_{ccvv}(\omega) = & \left\{ -i\left[-\omega_1 - \omega_2 + 2\left(-\frac{V_{cc}}{\hbar} + \omega_0\right)\right] \right. \\
& \left. - 2\gamma \right\} \rho_{ccvv}(\omega) - \frac{i}{2\sqrt{2}}[2\rho_{ccvc}(0) + 2\rho_{ccvv}(0) \\
& - \rho_{vc,2}(0)^* - \rho_{vc,1}(0)^*] \quad (\text{B9})
\end{aligned}$$

This system of linear equations can be solved analytically by using the following initial conditions.

(i) Without the pump pulse the system is in the ground state. All density matrix elements of the reduced system are zero at  $t=0$ .

(ii) With the pump pulse [of area  $\pi$ , renormalized according to Eq. (21)] the system is excited to the higher-energy

single-excitonic resonance  $|\Psi_3\rangle = (c_2|10\rangle + c_1|01\rangle)$ . The corresponding initial conditions are  $n_{c1} = |c_2|^2$ ,  $n_{c2} = |c_1|^2$  for the electronic densities and  $\rho_{ccvc} = c_1c_2^*$  for the density matrix elements. The remaining terms of the reduced system are zero initially.

Solving the system of equations for these two sets of initial conditions we obtain a solution for the polarization with and without the pump pulse from which the transmission spectra for both situations can be calculated. The difference, constituting the differential transmission spectra, is plotted for two situations calculated numerically in Sec. VII.

(i) No biexcitonic shift, strong Förster coupling (see Fig. 15). It can clearly be seen that with rising Förster matrix element an absorptive line occurs.

(ii) A biexcitonic shift of  $V_{cc} = 0.01$  meV, strong Förster coupling (see Fig. 16). One can see the occurrence of a dispersive line shape due to the biexcitonic shift and the fact that there is almost no difference between the spectra for the two different values of  $V_F$ . To show this effect more clearly, we plotted the spectra in a smaller region around the resonance (bottom).

These results correspond to the numerical evaluation for  $\Delta t \rightarrow +\infty$ , shown in Figs. 13 and 14.

- <sup>1</sup>D. Bimberg, M. Grundmann, and N. N. Ledentsov, *Quantum Dot Heterostructures* (Wiley, New York, 1999).
- <sup>2</sup>H. Haug and S. W. Koch, *Quantum Theory of the Optical and Electronic Properties of Semiconductors* (World Scientific, Singapore, 2001).
- <sup>3</sup>D. Loss and D. P. DiVincenzo, Phys. Rev. A **57**, 120 (1998).
- <sup>4</sup>S. C. Benjamin and S. Bose, Phys. Rev. Lett. **90**, 247901 (2003).
- <sup>5</sup>F. Troiani, E. Molinari, and U. Hohenester, Phys. Rev. Lett. **90**, 206802 (2003).
- <sup>6</sup>B. W. Lovett, J. H. Reina, A. Nazir, and G. A. Briggs, Phys. Rev. B **68**, 205319 (2003).
- <sup>7</sup>E. Biolatti, R. C. Iotti, P. Zanardi, and F. Rossi, Phys. Rev. Lett. **85**, 5647 (2000).
- <sup>8</sup>P. Borri, W. Langbein, S. Schneider, U. Woggon, R. L. Sellin, D. Ouyang, and D. Bimberg, Phys. Rev. Lett. **87**, 157401 (2001).
- <sup>9</sup>H. Htoon, T. Takagahara, D. Kulik, O. Baklenov, A. L. Holmes, and C. K. Shih, Phys. Rev. Lett. **88**, 087401 (2002).
- <sup>10</sup>A. Zrenner, E. Beham, S. Stuffer, F. Findeis, M. Bichler, and G. Abstreiter, Nature (London) **418**, 612 (2002).
- <sup>11</sup>A. Vagov, V. M. Axt, and T. Kuhn, Phys. Rev. B **66**, 165312 (2002).
- <sup>12</sup>E. Biolatti, I. D'Amico, P. Zanardi, and F. Rossi, Phys. Rev. B **65**, 075306 (2002).
- <sup>13</sup>L. Allen and J. H. Eberly, *Optical Resonance and Two-Level*

*Atoms* (Dover, Mineola, NY, 1987).

- <sup>14</sup>T. H. Stievater, X. Li, D. G. Steel, D. Gammon, D. S. Katzer, D. Park, C. Piermarocchi, and L. J. Sham, Phys. Rev. Lett. **87**, 133603 (2001).
- <sup>15</sup>H. Kamada, H. Gotoh, J. Temmyo, T. Takagahara, and H. Ando, Phys. Rev. Lett. **87**, 246401 (2001).
- <sup>16</sup>T. Unold, K. Mueller, C. Lienau, T. Elsaesser, and A. D. Wieck, Phys. Rev. Lett. **94**, 137404 (2005).
- <sup>17</sup>J. Förstner, C. Weber, J. Danckwerts, and A. Knorr, Phys. Rev. Lett. **91**, 127401 (2003).
- <sup>18</sup>B. Krummheuer, V. M. Axt, and T. Kuhn, Phys. Rev. B **65**, 195313 (2002).
- <sup>19</sup>E. Dekel, D. Gershoni, E. Ehrenfreund, D. Spektor, J. M. Garcia, and P. M. Petroff, Phys. Rev. Lett. **80**, 4991 (1998).
- <sup>20</sup>U. Woggon, *Optical Properties of Semiconductor Quantum Dots* (Springer, Berlin, 2003).
- <sup>21</sup>P. Y. Yu and M. Cardona, *Fundamentals of Semiconductors* (Springer-Verlag, Berlin, 1999).
- <sup>22</sup>T. Brandes, Phys. Rep. **408**, 315 (2005).
- <sup>23</sup>S. W. Koch, N. Peyghambarian, and M. Lindberg, J. Phys. C **21**, 5229 (1988).
- <sup>24</sup>T. Guenther, C. Lienau, T. Elsaesser, M. Glanemann, V. M. Axt, T. Kuhn, S. Eshlaghi, and A. D. Wieck, Phys. Rev. Lett. **89**, 057401 (2002).